Available online at www.sciencedirect.com
ScienceDirect
Trans. Nonferrous Met. Soc. China 32(2022) 2787−2813
Transactions of Nonferrous Metals Society of China
www.tnmsc.cn

Effect of extrusion parameters on degradation of magnesium alloys for bioimplant applications: A review

Mahdi SHIRI[1], Hassan JAFARI[1], Raman SINGH[2]

1. Materials Engineering Department, Faculty of Materials Engineering and Interdisciplinary Sciences, Shahid Rajaee Teacher Training University (SRTTU), 16785-136 Tehran, Iran;
2. Department of Mechanical & Aerospace Engineering and Department of Chemical Engineering, 17 College Walk (Bldg 31), Monash University-Clayton Campus (Melbourne), Vic 3800, Australia

Received 30 April 2021; accepted 31 May 2022

Abstract: Magnesium alloys, as a new generation temporary biomaterial, deserve the desirable biocompatibility and biodegradability, and also contribute to the repair of the damaged bone tissues. However, they do not possess the required corrosion resistance in human body fluid. Hot mechanical workings, such as extrusion, influence both the mechanical properties and bio-corrosion behavior of magnesium alloys. This review aims to gather information on how the extrusion parameters (extrusion ratio and temperature) influence the bio-corrosion performances of magnesium alloys. Their effects are mainly ascribed to the alteration of extruded alloy microstructure, including final grain size and uniformity of grains, texture, and the size, distribution and volume fraction of the second phases. Dynamic recrystallization and grain refinement during extrusion provide a more homogeneous microstructure and cause the formation of basal texture, resulting in improved strength and corrosion resistance of magnesium alloy. Extrusion temperature and extrusion ratio are reported as the influential factors in the degradation. The reports reveal that the increase in extrusion ratio and/or the reduction in extrusion temperature cause a decrease in the final grain size, leading to intensification of basal texture, in parallel side of the samples with extrusion line, and to lower volume fraction and size of precipitates in magnesium alloys. These all lead to improving the bio-corrosion resistance of the magnesium alloy implants.
Key words: magnesium alloys; extrusion temperature; extrusion ratio; biodegradation; microstructure

1 Introduction

Biomaterials are biocompatible substances that do not have a toxic effect on the organs and other parts of human body [1]. These materials are used as alternatives to living organs or tissues in human body as the therapeutic substances for the treatment of patients, and include materials such as metals and alloys, ceramics, polymers and composites [2]. Biomaterials used in the human body are shown in Fig. 1 [3].

Providing optimal mechanical properties, metallic implants are good substitute for the damaged bones. Primary metallic biomaterials generally undergo corrosion at low rates in physiological environment. Orthopedic implants are categorized as permanent joint replacements and temporary fracture fixation devices. Deficiency in finger joints, wrist, knee, ankle, shoulder, hip and elbow requires permanent implants. These implants are designed to serve in the patients' body throughout their whole life. On the other hand, the temporary implants serve for a relatively short time, and once the damaged bones are healed, the implants can be removed. Intramedullary nails, plates,

Corresponding author: Mahdi SHIRI, Tel: +98-9371514491, E-mail: mahdi_shiri@yahoo.com, ORCID: 0000-0003-4082-3266;
Hassan JAFARI, Tel: +98-2122970022, E-mail: hjafari@sru.ac.ir
DOI: 10.1016/S1003-6326(22)65984-3

screws, pins, and wires fall in this category [4]. After the regeneration of the damaged bone tissues, the temporary implant must be surgically removed from the body [5]. Implants of commonly used materials (such as stainless steel, cobalt−chromium, titanium, and nickel alloys) might be corroded by body fluid or worn out, and leave some debris in human body. Such residual substances may have cytotoxic effects on the nerve tissues and cells [6,7].

According to the classification of CHEN and THOUAS [5], biomaterials are divided into three different generations (Table 1). The first generation is relatively well-adapted to the human body and has an almost neutral effect on the human body. The second generation has been developed with therapeutic properties and relative improvement of damaged tissue. Vascular stent, one of the widely used biometals, is among this generation. The third generation, such as magnesium, in addition to having the properties of previous generations, is electrochemically active in the physiological environment. In other words, such materials, after healing the damaged organs, are harmlessly dissolved away in the body [8], and they do not require to be removed from human body by extra surgeries [9].

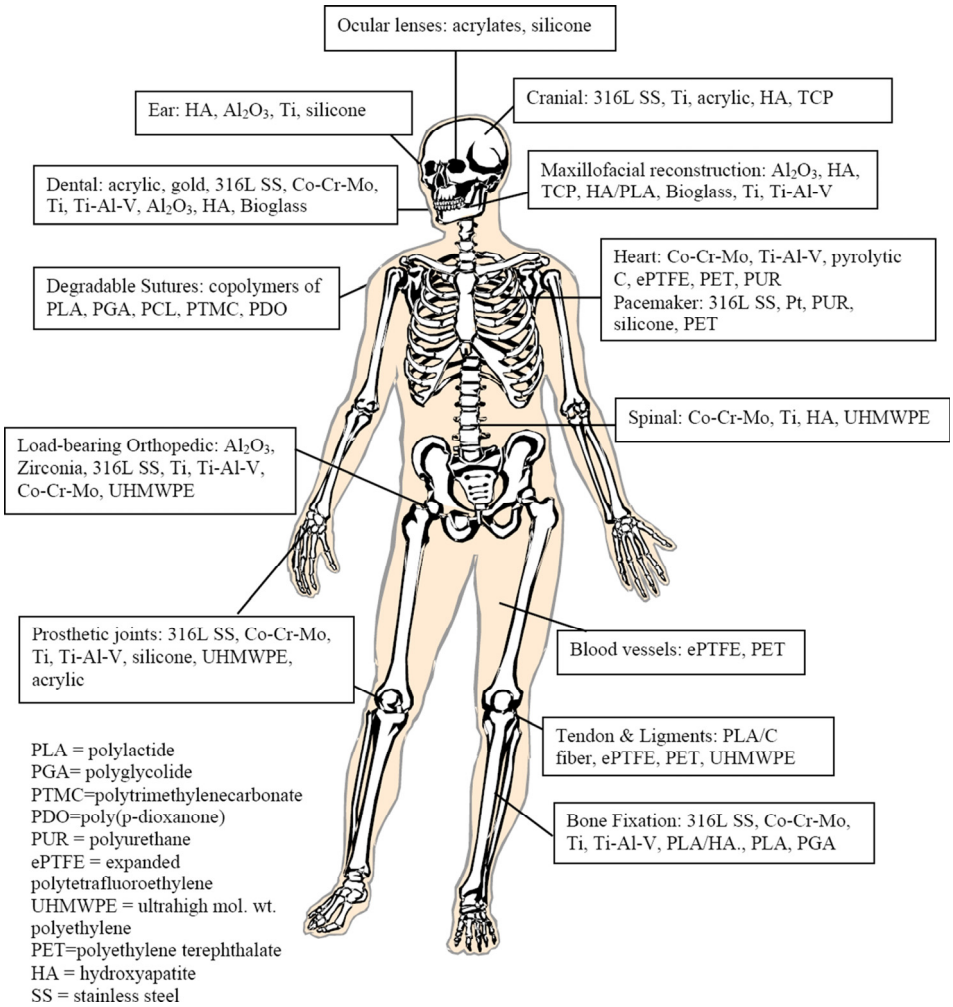

Fig. 1 Various biomaterials used in human body [3]

Table 1 Generations of biomaterials [5,8]

Generation (inception period)	Goal	Biomaterial
First (1950−1960)	Bioinert	Cobalt alloys, Al_2O_3, polyurethane
Second (1980− 2000)	Bioactivity	Titanium alloys, hydroxyapatite, calcium phosphate, surface bioactive glasses
Third (2000−)	Regenerate functional tissue	Magnesium alloys, degradable bioglass degradable polymers

The first and second generations of metallic biomaterials (such as iron, chromium, cobalt, nickel, tantalum, niobium, molybdenum and tungsten) have lower compatibility with the physiological environment compared to those in the third generation. It should be noted that, in some cases, they are rejected by the human body and require extra surgeries for their incorporation, repair, and then removal from the body. In some cases, the wear or corrosion products of these materials have allergic effects on the surrounding tissues, and sometimes, may even bring about a toxic and infectious effect on the surrounding cells (such as debris produced by corrosion of Ni−Co−Cr alloys) [5,6]. An increase in nickel content of stents constructed out of this alloy has shown a toxic effect due to the degradation product [10]. Similarly, the corrosion product debris of titanium implant accumulate in surrounding tissues and cause detrimental effects [7]. Also, titanium alloy, due to its high elastic modulus, has a stress shielding effect on the damaged bone, which increases the load on the repaired bone [5,11]. In contrast, magnesium alloys provide an increased healing rate of damaged bone [12] while do not inflict much stress shielding.

Yet, magnesium is severely degraded in the physiological environment (pH ~7) which is a critical concern about its applicability as implants [13−15]. Such degradation also compromises its mechanical strength decrease [16]. Also, hydrogen gas is produced due to the cathodic reaction in magnesium corrosion [17]. Spreading into loose structures, the gas results in subcutaneous emphysema, and the continuous evolution of the gas and its accumulation generate bulbs in the body, which cause discomfort and disturb the balance of blood cell parameters. This fact increased the mortality rate of rats which were used for in-vivo experiments [18]. Therefore, before magnesium and its alloys could be effectively employed as bioimplants, it is necessary to address the concerns about their electrochemical properties and strength during their exposure to the physiological environment. Common approaches to address such concern are alloying with suitable elements, heat treatment, and coating [19−21]. In addition to alloying and solid solution strengthening, the strength of magnesium alloys can be further enhanced by hot mechanical working [22−24]. Among the various mechanical working approaches, extrusion has provided optimal properties, and in comparison to alloying, has much greater effect on the grain refining, final strength and yield strength of the alloy [24]. PENG et al [25] reported that both mechanical properties and corrosion resistance of as-cast Mg−2Zn alloy are significantly improved. Some reports suggest that the extrusion process also improves corrosion resistance of magnesium alloys, and the corrosion rate of the alloy depends on the extrusion parameters, such as temperature and extrusion ratio [26−29]. Therefore, this study aims to present a comprehensive and critical review of the effects of extrusion ratio and extrusion temperature on corrosion performances of magnesium alloys.

2 Magnesium biomaterials

Due to its degradability in the physiological environment, the required specific strength, and the closer mechanical properties to the bone, magnesium has been studied extensively as a temporary bioimplant material in recent years. This metal possesses ideal biocompatibility and plays a key role in the chemical process of the body. Moreover, about 53% of the body's magnesium deposits in the bone marrow. In addition, this metal possesses an ideal biocompatibility. However, magnesium suffers from corrosion at an unacceptably high rate in the aqueous chloride environment such as human body fluid, which is a major obstacle in its effective use as an optimal implant [13,14].

As seen in Table 2, magnesium alloys, compared to the traditional biomaterials, have similar properties to bone, namely density, strength, and modulus to bone [5]. These alloys are also much cheaper than traditional implant alloys [31]. Magnesium surface when exposed to body fluid develops calcium phosphate, i.e., one of the main constituents of bone [32]. Zn and Mg are essential elements for having a healthy body and offer high biocompatibility; yet, Zn is a less preferable option over Mg since the recommended daily consumption of Zn for an adult is up to 11 mg/d, while this amount for Mg is up to 420 mg/d. Also, compared to other biomaterials including Zn and Fe, the elastic modulus and density of Mg are much closer to those of a natural bone [21].

Table 2 Comparison of mechanical properties of biometals and cortical bone [5,21,30]

Material	Elastic modulus/GPa	Ultimate tensile strength/MPa	Fracture toughness/(MPa·m$^{1/2}$)
Cortical bone	10−30	120−150	2−12
Mg alloys	40−45	100−250	15−40
Ti alloys	105−125	900	~80
CoCrMo alloys	240	900−1540	~100
316L stainless steel	200	540−1000	~100
NiTi alloy	20−50	1355	30−60
Fe-based alloys	200−205	210−360	−
Zn-based alloys	90−100	160−390	−

According to an in-vivo research [33], the degradation of implanted magnesium brought about minor changes to blood composition after 6 months and had no adverse physiological effects on organs, such as liver and kidney. Magnesium was first used in 1878 as a suture thread. The history of magnesium biomaterial is summarized in Table 3 [34]. Some of the magnesium implants used in the physiological environment are shown in Fig. 2.

As described earlier, magnesium alloys are very attractive as an alternative to the damaged hard tissues in the body, such as bone. However, magnesium and its alloys degrade too rapidly in human body fluid, and this rate needs to be slowed down for controlled decomposition in order for their mechanical properties to be maintained for the required period of time [35,36].

3 Corrosion of magnesium biomaterial

Corrosion in the physiological environment usually has galvanic and pitting nature [37,38]. Corrosion of magnesium in the physiological environment is caused by anodic (Eq. (1)) and cathodic (Eq. (2)) reactions, as shown in Fig. 3 [39]. With cathodic reaction, the pH of the solution increases, which facilitates the stabilization of the $Mg(OH)_2$ passive film. Magnesium can undergo both internal galvanic corrosion and external galvanic corrosion. When adjoined to a metal with more positive potential, magnesium acts as anode, and external galvanic corrosion occurs. On the other hand, the secondary phases and/or inclusions that exist in magnesium alloy matrix, are often cathodic to the main alloy matrix, and they can cause local galvanic corrosion to the adjoining anodic matrix. This represents internal galvanic corrosion. The external and internal galvanic corrosion mechanisms are schematically shown in Fig. 4 [40].

$$\text{Anodic reaction: } Mg \rightarrow Mg^{2+}+2e \quad (1)$$

$$\text{Cathodic reaction: } 2H_2O+2e \rightarrow H_2\uparrow+2OH^- \quad (2)$$

Corrosion of magnesium, like other metals in the electrolyte with constant potential is a function of pH, and can be investigated under equilibrium conditions [37]. A combination of Pourbaix diagram for magnesium metal and various environments inside the body is shown in Fig. 5 [2]. Magnesium with standard electrode potential of 2.372 V (vs SHE) is known as a low corrosion resistance element [5]. Also, some of the measured corrosion rates (CR) of pure Mg and its alloys are listed in Table 4.

The high corrosion rate of magnesium alloys in the physiological environment is detrimental to the practical aim of repair of the damaged bone tissues; it takes at least 3−6 months for the damaged bone tissue to fully recover and return to the healthy state. The estimation of bone healing time for different fractures is stated in Table 5 [52]. Therefore, during this period, it is necessary that the used biomaterial, in addition to maintaining the strength, provides a good corrosion resistance, and suffers any significant degradation only after the formation of bone tissue. But, most of the magnesium biomaterials are completely degraded within four months of implantation [52].

Furthermore, bio-implants are under various load and stress patterns in human body, as dictated by the location they are placed at. The combination of mechanical loading and the corrosion can also cause stress corrosion cracking (SCC) and corrosion fatigue (CF), which can bring

Table 3 History of application of magnesium alloys as biomaterial [34]

Year	Magnesium (alloy)	Application	Human/animal model	Result of implantation
1878	Pure magnesium	Wires as ligature	Humans	Successfully stop bleeding vessels
1892−1905	High-purity magnesium	Tubes (intestine, vessel, nerve connector), plates, arrows, wire, sheets, rods	Humans, guinea pigs, rabbits, pigs, dogs	Intravascularly placed Mg tubes exhibited thrombotic blood clotting
1903	Pure magnesium	Magnesium cylinders as vessel connectors	Dogs	Observing thrombosis in vessels with a diameter less than 3 mm
1900−1905	High-purity magnesium	Tubes, sheets and cylinder intestine connector, arthoplastik	Humans, rabbits, dogs	Sheets were completely corroded after 18 days
1906−1932	Pure magnesium (99.7%)	Rods, plates, screws	Humans, rabbits, dogs	Human body experienced extensive subcutaneous gas cavities, local swelling and pain after implantation of Mg plate with six steel screws at the tibia
1910	Metallic magnesium	Ring-plates for anastomosis	Dogs	Rings were tied firmly together, but not so tight as to cut the intima and cause vessel necrosis
1917	Pure magnesium, mix. of eq. part: Mg/Al, Mg/Cd, Mg/Zn	Wires, clips as ligature, anastomosis	Dogs	Cannot be tied in even loose knots, as it breaks immediately on kinking
1924	Pure magnesium (99.99%), distilled in vacuum	Wires, strips, bands	Rabbits	Wires had a low tensile strength and were not sufficiently pliable
1925	Pure magnesium (99.8–99.9%)	Magnesium arrows	Humans, rats, cats	Mg arrow therapy may not be beneficial for large and not purely cavernotic haemangioma
1928	Pure magnesium	Magnesium arrows	Rabbits	Mg corroded quickly in haemangioma, which leads to the early transformation of the haemangioma into a fibrous granulation tissue
1933−1937	Dow metal: Mg−Al6−Zn3−Mn0.2 wt.% Elektron Mg−Al8wt.%	Plate, band, screws, pegs	Humans, dogs, rats, rabbits	All patients experienced regular body temperatures; while the skin, soft tissue, bone and joints showed no adverse reactions to the corroding magnesium
1938	Mg−Mn3wt.%, Mg−Al4−Mn0.3wt.%	Sheet, plate, band, screw, peg, wire	Humans, dogs	Screws were more resistant to corrosion than plates, especially when the screws were fitted more tightly into hard cortical bone
1939	Elektron (alloy not specified)	Rods	Rabbits	The gas evolution due to the corrosion led indirectly to slight bone damage
1948	Mg−Cd	Plate, screws, rod-plate	Humans	successful treatments of 34 cases of pseudarthrosis with a plate and screw combination
1940	Magnesium	Band, suture from woven Magnesium wires, fusiform pins	Humans, rabbits	Corroding the Mg and the formation of gas cavities, as well as extensive periostal bone formation
1951	Mg−Al2wt.% pure magnesium	Wires for clotting aneurysms	Dogs	Mg−Al alloy wires were twice as thrombogenic as stainless steel
1975	Ind.-grade purity: Domal magnesium (99.9%), T.L.H. Mg not reported Lab-grade purity: ‘‘zone fondue” Mg, R69 Mg, MgMn1.5wt.%, MgAl: GAZ8%, GAZ6%, GAZ3%	Anodes for implantable batteries to feed pacemaker	Dogs	Domal magnesium (99.9%) was superior to the Mg−Mn alloy due to the possible toxicity of manganese, while both alloys did not show any subcutaneous necrosis
1980	Mg−Al2wt.%	Wires intravascular	Rats	Wires dissolved within 2 weeks and caused an increase in adrenal glandular weight, thymic involution, depression of the abnormally elevated blood pressure and a retarded gain in weight
1981	Pure magnesium (99.8%)	Wires for hemangioma treatment	Rats, rabbits	Very mild foreign body reactions around the corroding Mg wires, and the structure and function of the neighbouring nerves and muscle fibers were preserved
1981	Pure magnesium (99.8%)	Wires for Hemangioma treatment	Humans	A good clinical result was obtained in 50% of the cases, since various types of haemangioma were treated. No adverse effect was observed in a 5-year follow-up

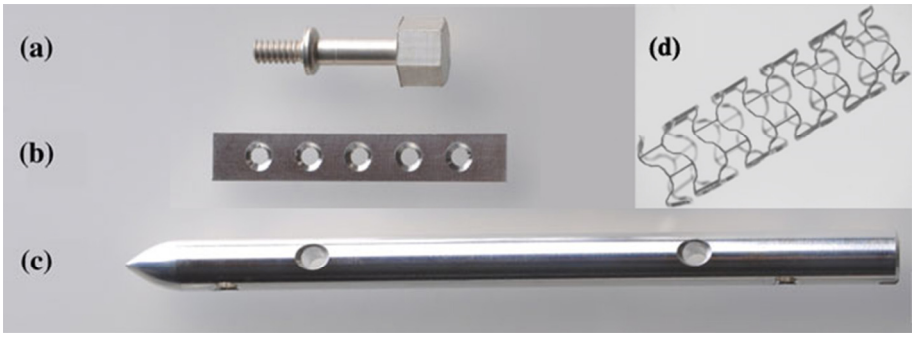

Fig. 2 Magnesium implants: (a) Mg−0.8wt.%Ca screw; (b) ZEK100-plate; (c) Intramedullary LAE442-nail; (d) WE43 stent [21]

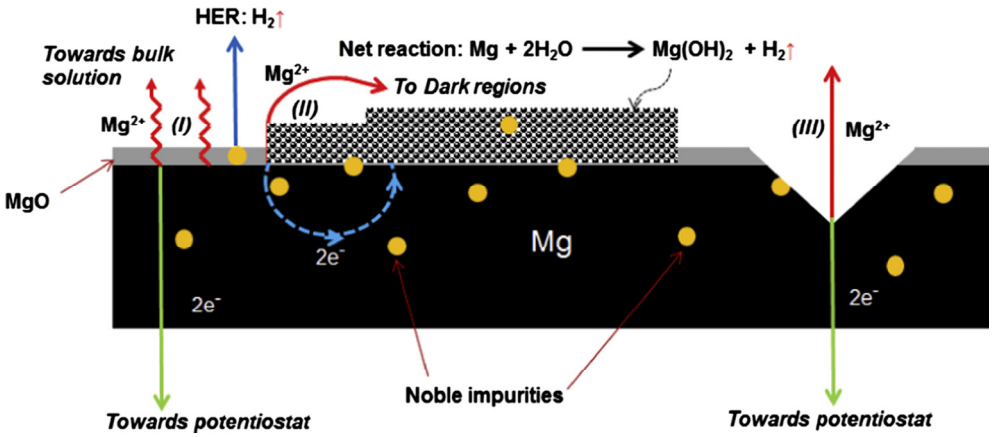

Fig. 3 Corrosion mechanism of immersed magnesium alloy in solution (During anodic polarization, Mg^{2+} ions released into solution may remain soluble and diffuse towards the bulk solution (I). A fraction of the Mg^{2+} ions transform into the insoluble form, $Mg(OH)_2$, by undergoing the net reaction (II) (while inside the human body that has high concentration of chloride ions, $Mg(OH)_2$ is soluble). Hydrogen is evolved during one of the reaction steps. Sudden spikes of Mg^{2+} ions may be released into solution, during sudden ‘‘breakdown’’ of the intact MgO-based film (III)) [39]

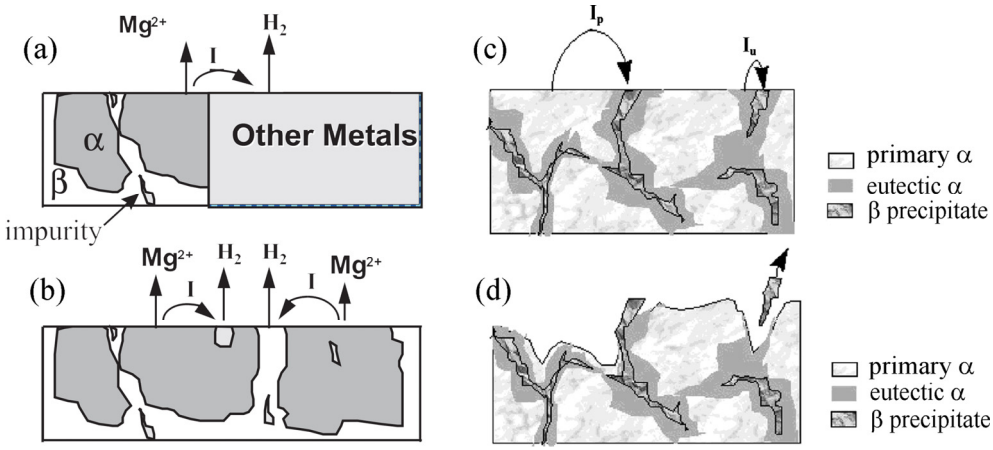

Fig. 4 External galvanic corrosion (a), internal galvanic corrosion (b), galvanic corrosion of primary α and eutectic α (c), and final corrosion morphology (d) [40]

about premature cracking of implants [53−55]. Magnesium alloys offer lower fatigue resistance than traditional biometals [30]. Therefore, an alloy must be developed to provide optimal resistance to corrosion and corrosion-assisted cracking. To address this requirement, various approaches such as suitable alloying and purification [56−59], surface engineering and coating [60−62], heat treat-

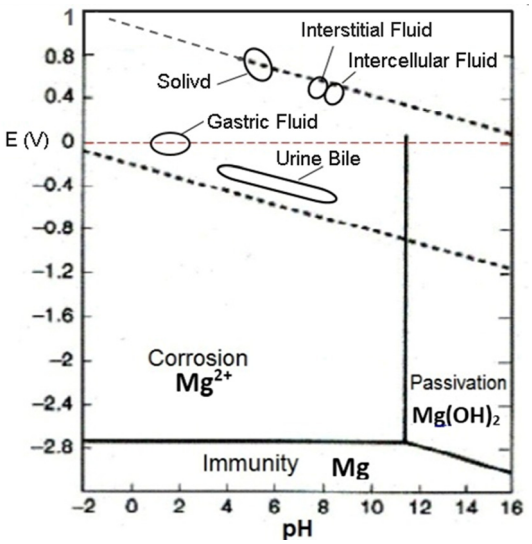

Fig. 5 Pourbaix diagram showing regions of different electrochemical behaviors of magnesium alloys, including in various body fluids [2]

Table 4 Bio-corrosion rate of different Mg-based alloys

Alloy	Solution	CR/(mm·a^{-1})	Ref.
Pure Mg	Minimum essential medium (MEM)	0.440	[41]
Pure Mg	Kokubo solution	2.184	[19]
As-cast ZK60	Simulated body fluid (SBF)	0.532	[42]
As-cast AZ31	SBF	1.114	[43]
As-cast AZ91	SBF	0.110	[44]
As-cast AZ91	SBF	0.632	[45]
As-cast Mg−4Zn	SBF	1.720	[46]
As-cast Mg−3Zn−0.4Ca	Hanks solution	2.190	[47]
As-cast Mg−1Zn−1Ca	Hanks solution	1.290	[47]
As-cast Mg−Zn−Y−Nd	SBF	3.122	[48]
Extruded AZ31B	SBF	3.100	[49]
Extruded LAE442	in-vivo (Rabbit femur)	0.310	[50]
Extruded Mg−Nd−Zn−Zr	Artificial plasma	0.337	[51]

ment [63,64], and hot or cold mechanical working [65−67], have been employed. Among these, hot mechanical working offers an implant with both higher strength and greater corrosion resistance simultaneously; however, this is not a general rule, as there are many exceptions that thermomechanical working results in lower strength and corrosion resistance due to the textural evolution and the presence of defects.

Table 5 Healing time for different fractures of bones in human body [52]

Fracture	Healing time/week	Fracture	Healing time/week
Clavicle	5−7	Pelvis	6−10
Fingers	4−8	Femur	8−14
Scaphoid	>10	Neck of femur	12−24
Humerus	5−8	Tibia	8−12
Radius and ulna	8−12	Calcaneus	6
Distal radius	3−4	Toes	6−8

4 Hot mechanical working on magnesium

One of the critical approaches to improve strength of alloys is the mechanical working (hot or cold). Using this method, the deleterious effects of heat treatment, such as increasing grain size, can be greatly circumvented [68]. Despite its high cast-ability, magnesium metal has a poor formability at ambient temperature, which is due to the hcp crystal structure. However, magnesium alloys attain high strengths after forging, hot and cold rolling, extrusion, and compression [65,69−71]. Among these processes, the hot extrusion of magnesium, due to the lack of metal loss during mechanical work, has gained the attention of many researchers [72,73].

In pure magnesium and at temperatures below 225 °C, slip only occurs on the basal planes. Also, the twinning phenomenon contributes to the deformation of magnesium. However, magnesium deformation is difficult at ambient temperature, and during cold deformation of magnesium, the probability of local stress concentration and fracture is very high. At higher temperatures, the additional slip systems (known as non-basal slip systems) are activated in magnesium and the plasticity of the alloys is greatly increased. Non-basal slip systems include the prismatic ⟨*a*⟩ and pyramidal slip ⟨*c*+*a*⟩ systems [74].

The activity of these systems (critical shear resolved stress or CRSS) depends on the soluble atoms, secondary phases or precipitates and temperature. The experimental values of CRSS for

basal planes, extension twinning planes, prismatic planes, first-order and second-order pyramidal planes of the single-crystal magnesium are 5, 10, 20, 40, and 70−80 MPa, respectively. As the temperature increases, the CRSS in the prismatic system decreases sharply, the mobility of the screw dislocations increases, the formability of magnesium alloys improves, and the probability of mechanical fracture greatly reduces [72,74,75]. One of the important effects of thermomechanical processes in metals is the activation of static and dynamic restoration mechanisms in the metal because of high strain rates (10^{-3}−10^{3} s^{-1}). Due to the low stacking-fault energy (SFE) in magnesium alloys, the duration of dynamic recovery (DRV) is short in these alloys, and at temperatures above 240 °C, dynamic recrystallization is also observed in the alloy. However, at temperatures greater than 360 °C, dynamic recrystallization is the predominant mechanism. During magnesium thermomechanical process, first, dynamic recovery and lots of twinning are produced, but by increasing the process temperature (more than 200 °C) and as a result of activation of the pyramidal slip system, the twinning also decreases [76].

The microstructure of magnesium alloys, under the influence of restoration mechanisms, changes the properties of the alloys such as corrosion and strength. For instance, after the extrusion process on a magnesium alloy, the rate of anodic and cathodic reactions decreased and the corrosion rate of the extruded alloy reduced significantly compared to the as-cast alloy, but with additional mechanical work (rolling after the extrusion), the corrosion resistance of alloy deteriorated [77]. XIA et al [78] implanted the extruded magnesium−zinc−calcium alloy inside the body, and after 3 months observing that 35% of this alloy was degraded, and structures similar to bone tissue were formed on the surface of alloy.

In general, it can be said that any kind of additional treatments after casting, including heat treatment, hot and cold mechanical work, etc., as well as changing the parameters of hot working, such as extrusion ratio or temperature, have special effects on the final structure, strength, flexibility, hardness, and corrosion resistance; however, suitably optimized mechanical working, especially extrusion may still be one of the best ways to improve the corrosion resistance of magnesium implants [79,80].

5 Extrusion of magnesium alloys for bioimplant application

Direct and indirect extrusions are common and traditional types (Fig. 6). Usually, before the extrusion, homogenization process is performed on magnesium alloys, particularly in the case of high speed extrusion. Magnesium alloys are often deformed using direct extrusion. Although the indirect method requires lower forces (due to the reduction of friction between sample and mold) and the deformation ratio increases, the formability of magnesium with different diameters is limited in this method. Magnesium alloys are also extruded by other modern methods such as equal channel angular extrusion (ECPE), cold extrusion, and

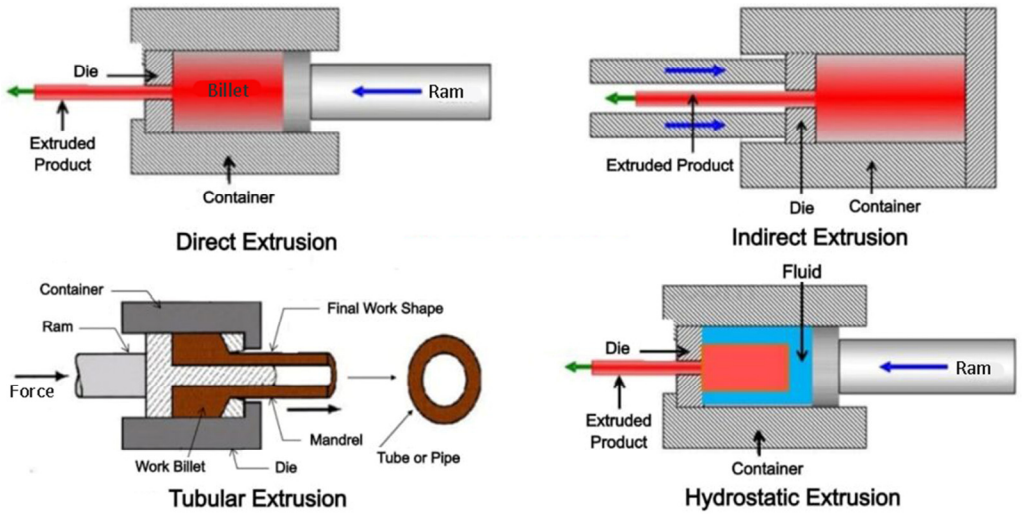

Fig. 6 Types of extrusion [81]

hydrostatic extrusion. In terms of the extrusion operation, the force used for extrusion depends on variables such as extrusion type, temperature, extrusion ratio and extrusion speed, and the friction of metal and mold [72,73].

The extrusion ratio (R) is the ratio of the initial cross-sectional area (A_0) to the final cross-sectional area (A_f) after the extrusion [82]:

$$R = \frac{A_0}{A_f} \tag{3}$$

Extrusion velocity is equal to the speed of stem and dummy block, which determines the deformation rate. Extrusion temperature is the temperature of the die, billet and extrusion container during the process. As the temperature increases, the flow stress decreases. Therefore, usually a high temperature process is employed for the extrusion; so, the deformation resistance of alloy decreases with increasing temperature. In the high temperature extrusion process, it is possible to reduce the amount of required force and increase the rate of the process.

Friction is also an effective factor on the applied force in extrusion process. The smoothness of the interior surfaces of the container and die, as well as the angle of the die is effective factor in the friction between the billet and the mold. Therefore, it is necessary to use a lubricant to reduce the friction during the process. Also, in order to decrease the dead zone during extrusion and increase the material flow inside the extrusion die, a die with a conical angle is used.

In general, the effects of extrusion process on the final properties of magnesium alloy are due to microstructural changes in the alloy [77,83,84].

5.1 Grain size and secondary/deposited phases influences on corrosion of extruded Mg alloys

WU et al [85] reported that after applying the extrusion process on the Mg−Zn−Y−Nd alloy at the temperature of 270 °C and extrusion ratio of 25:1, the corrosion performance of the alloy in the simulated body fluid (SBF) improved. Although, dynamic recrystallization (DRX) did not occur completely, the grain size was decreased and the structure became more homogeneous. Both as-cast and as-extruded samples had the same corrosion mechanisms, but the corrosion rate in the immersion test and the corrosion current density in the polarization test were reduced, as seen in Fig. 7.

It has been generally proved that the corrosion properties of magnesium alloys are improved after grain refining. LU et al [86] reported that the bio-corrosion rate increases with increasing grain size in the alloy due to minimizing the segregation in the alloy, while its corrosion behavior is more homogeneous in a fine-grained microstructure. In another study, the direct relationship between grain size and the corrosion rate is declared [87]. Accordingly, as a result of grain refining and the presence of high misorientation angle grains, corrosion resistance of the magnesium alloy is improved, since these two factors promoted a more coherent oxide on the immersed alloy surfaces.

In another study [88], after the extrusion process at 350 °C with the extrusion ratio of 25:1 on the as-cast Mg−5wt.%Ca alloy, it was observed that the initial brittle and continuous secondary phases were completely crushed and arranged in the longitudinal direction of as-extruded alloy in the alloy matrix (Fig. 8). The secondary phase of Mg_2Ca has the corrosion potential of −1.54 V (vs

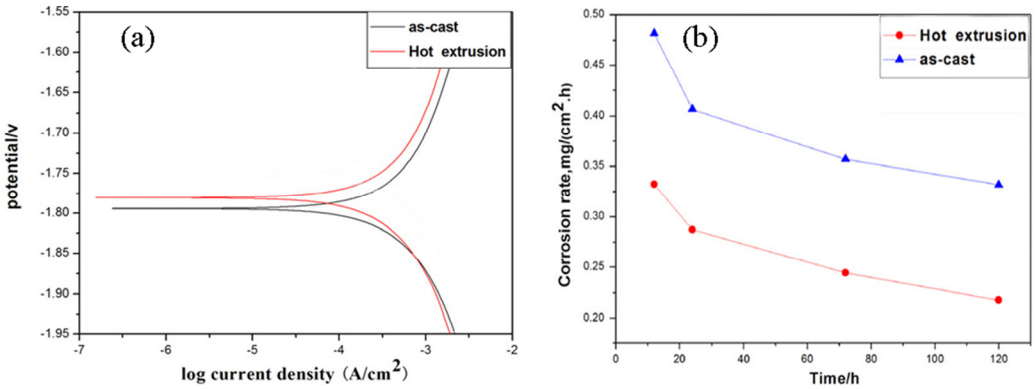

Fig. 7 Potentiodynamic polarization curves of Mg−Zn−Y−Nd alloy (a), and corrosion rate curves of Mg−Zn−Y−Nd alloy with immersion time in SBF solution at 37 °C (b) [85]

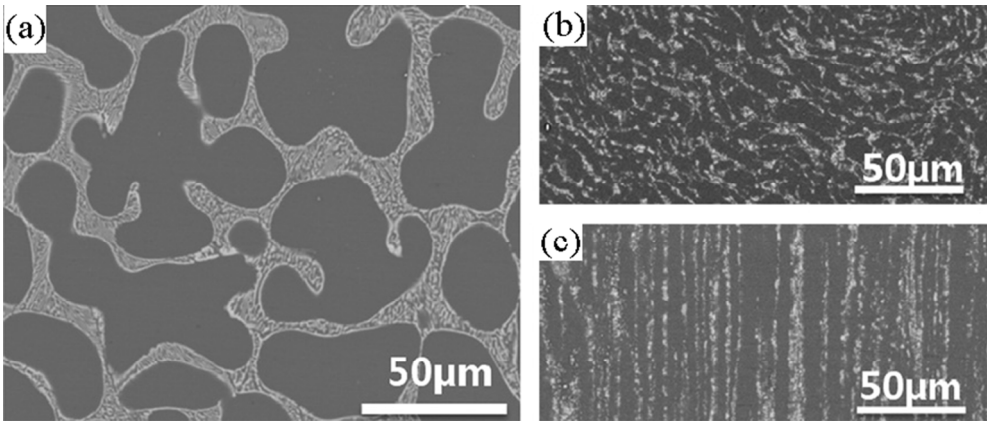

Fig. 8 SEM images of Mg–5Ca alloy: (a) As-cast; (b) Longitudinal direction of extrusion; (c) Radial direction of extrusion [88]

SHE) and the matrix phase has the potential of −2.37 V (vs SHE), which led to the formation of internal galvanic couple in the structure. Since the surface exposure of the cathodic precipitates is greater in the as-cast alloy than that in the extruded alloy, the corrosion rate is greater for the as-cast alloy. For the same reason, the amount of released hydrogen (i.e., concurrent with magnesium corrosion) is the least in the radial direction of the extruded sample, followed by the longitudinal direction, and it is the highest for the as-cast alloy (Fig. 9).

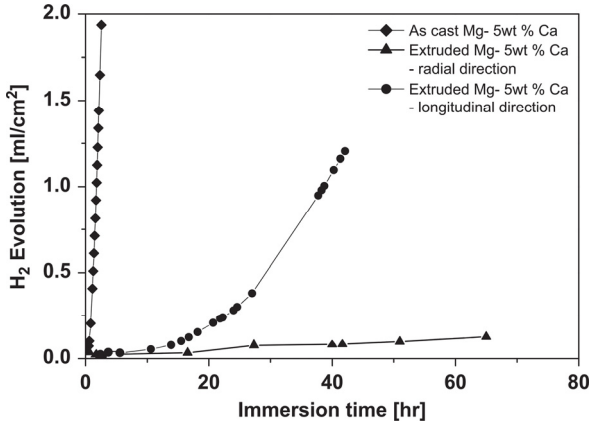

Fig. 9 Hydrogen evolution rates of as-cast and extruded Mg−5Ca alloy in SBF [88]

The bio-corrosion rate increases with the rise of the volume fraction of secondary phases because of the galvanic corrosion developed between the cathodic (secondary phase) and the anodic (magnesium matrix) regions [86].

5.2 Microstructural heterogeneities (dislocations, twinning, shear bands) influences on corrosion of extruded Mg alloys

As the number of dislocations and twins increases, corrosion rate grows up drastically [89]. In this regard, ZHENG et al [90] reported that due to the cold tensile deformation of the Mg−3Zn alloy, the number of dislocations increases, and by applying cold compressive deformation, the number of twinning increases. Due to the increase of the twins and dislocations, the residual stress in these zones rises, which causes an increase in corrosion rate of the alloy in the Hanks solution. HAMU et al [91] studied the relationship of the microstructure of AZ31 alloy after extrusion with corrosion in the 3.5% NaCl solution (pH, 10.5). The mechanical work performed on this alloy included direct extrusion with a ratio of 91.34% (ER91) and equal channel angular extrusion (ECAE) with a ratio of 98.99% (ER98) at 350 °C. After extrusion, the grain size was reduced by almost the same percentage for both ER91 and ER98 samples. The grain sizes of the as-cast, ER91, and ER98 samples were 29−35, 12−24 and 9−14 μm, respectively. Extrusion not only led to the enhancement of the dislocations density in this alloy, but also greatly increased the grain boundary length-density. In contrast, ECAE process, in addition to reducing grain size and severely enhancing dislocations density, has also greatly increased the amount of twinning. This indicates an incomplete DRX in the final microstructure of alloy. Therefore, as suggested through the polarization curves (Fig. 10(a)), the corrosion rate is severer in ER98

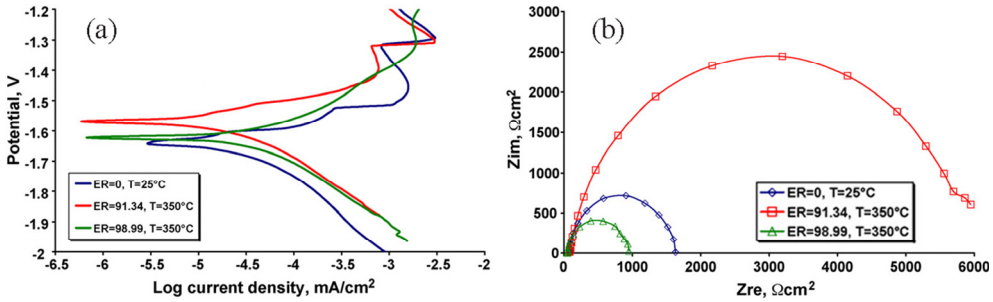

Fig. 10 Potentiodynamic polarization curves of AZ31 magnesium alloys with different extrusion ratios (ER) (a), and Nyquist plots of alloys (b) [91]

alloy than the extruded ER91. The Nyquist plots (Fig. 10(b)) also suggest the same corrosion mechanism for all three samples.

5.3 Texture influence on corrosion of extruded Mg alloys

The final texture of alloys with hexagonal structure, in addition to creating anisotropic characteristics and directional mechanical properties, also affects the corrosion properties. After the hot extrusion, the usual texture of magnesium is the basal (placing planes {0001} parallel to the longitudinal direction of extrusion), which is profoundly governed by the temperature and dynamic precipitates (precipitates formed during hot extrusion due to the presence of high-energy sites such as dislocations in DRXed microstructure). Cold mechanical working of Mg alloys decreases the texture intensity; however, alloys that extruded at 150−250 °C exhibit the maximum basal texture, and a further increase in extrusion temperature leads to the formation of dynamic precipitates which develop weaker basal texture [92]. Final structures with strong basal texture that has no twins, offer better corrosion resistance in comparison to that with fiber texture (a fiber texture is present with a maximum at the {1010} position) or mixed basal + fiber texture [93,94]. JIANG et al [95] confirmed that the greater the intensity of basal plane, the lower the corrosion rate of as-extruded magnesium alloys.

6 Effect of extrusion on corrosion of magnesium alloy

As mentioned earlier, extrusion process has different effects on the final microstructure, and therefore, on the final properties of the magnesium alloy. Corrosion of as-cast Mg−1.5Y−1.2Zn−0.44Zr alloy which was solution treated and extruded, was investigated [96]. The alloy was solution treated at 450 °C for 10 h, and then extruded at 350 °C with the extrusion ratio of 16:8. According to Fig. 11, the mass loss is the same for all samples in the first 24 h of immersion in the solution, but upon increasing the immersion time, the mass loss rate for the extruded sample is the lowest and the solution in which the extruded sample was immersed has the lowest pH (about 8.2).

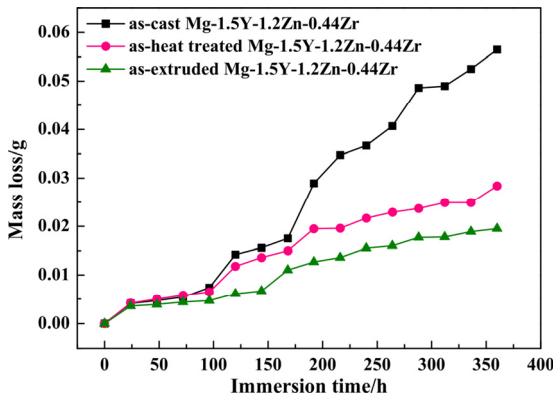

Fig. 11 Mass loss of as-cast, heat treated and extruded Mg−1.5Y−1.2Zn−0.44Zr alloy during immersion for 400 h in SBF [96]

After the solution treatment, the volume fraction of secondary phases was reduced in the structure and the grains became more homogeneous, but the grain size increased a little. After extrusion, the grain size reduced and the residual secondary phases became fine and scattered along linear bands parallel to the extrusion axis. The grain sizes of the as-cast, solid solutionized and extruded samples were 32, 37 and 10 μm, respectively, and the

extruded sample exhibited the best tensile strength and elongation. The corroded surfaces of the as-cast and solid solution samples had wide cracks with a greater depth compared to the extruded sample. The film formed on the surfaces of as-cast and solid solution samples is thicker than that on the extruded sample. The polarization diagram and the Tafel curves of the samples (Fig. 12(a)) indicate the reduction in the current density (i.e., increase in the corrosion resistance) for the extruded sample. The Nyquist plots indicate the corrosion mechanism to be similar for all three samples (Fig. 12(b)). However, the corrosion rate is the lowest for the extruded alloy.

ZHOU et al [97] reported that upon extrusion (with ratio of 14:7 at 350 °C and velocity of 4 mm/s), the grain size of Mg−1Mn−2Zn−1Nd alloy was reduced from 155 μm to 2−8 μm, and more homogeneous grains were formed in the alloy. According to Fig. 13(a) extrusion also vastly improved the corrosion resistance. The Nyquist plots (Fig. 13(b)) suggest the similarity of corrosion mechanism for both as-cast and extruded samples; however, consistent with the polarization results, the corrosion rate of the extruded alloy is lower than that of the as-cast alloy.

Most of the studies on the effect of extrusion on corrosion have shown extrusion to improve corrosion resistance; however, there are a few studies where opposite effect has been found. In a previous study [98], the corrosion of a Mg−Nd−Zn−Zr alloy after extrusion was examined. The magnesium billet was turned into a tube upon extrusion and severe deformation. The grain size in the radial direction of extrusion was reduced from 25−35 μm to 10−20 μm. A heterogeneous microstructure (elongated grains, shear bands, etc.) was created in the alloy, and continuous secondary phases, which were created during the casting in the structure, spread and scattered in tiny forms after the extrusion. The immersion corrosion rates of as-cast and extruded alloys in the 5% NaCl solution were 0.203 and 0.232 mg/(cm^2·d), respectively, indicating an increase of the corrosion rate after extrusion. This observation is in contrast to the commonly reported improvement of corrosion

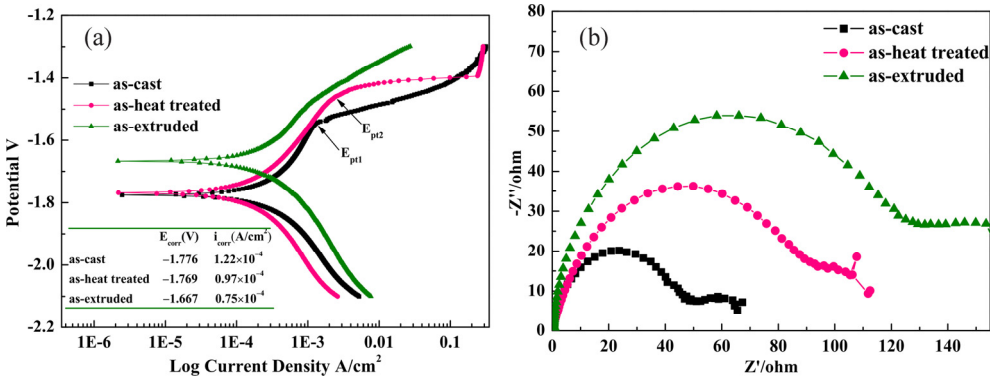

Fig. 12 Nyquist plots of as-cast, heat treated and extruded Mg−1.5Y−1.2Zn−0.44Zr alloy in SBF (a), and their potentiodynamic polarization curves (b) [96]

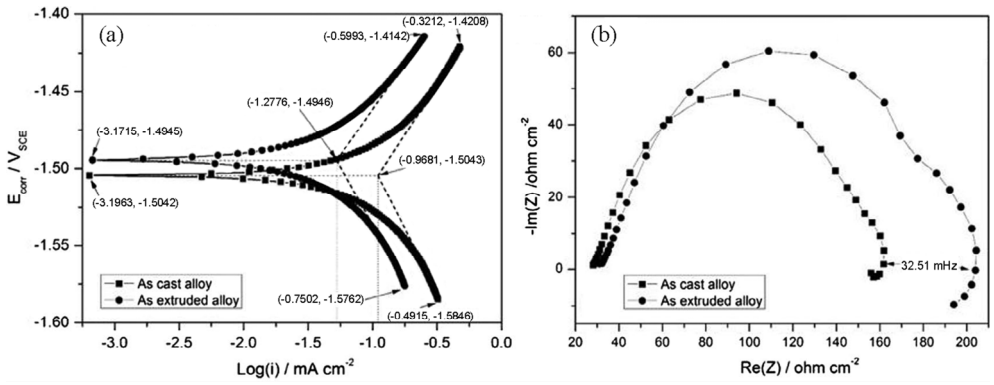

Fig. 13 Electrochemical measurement of as-cast and extruded Mg−1Mn−2Zn−1Nd alloy in SBF: (a) Nyquist plots; (b) Polarization curves [97]

performance of magnesium alloys upon extrusion. The extrusion parameters may be responsible for the opposite nature of effects. Accordingly, the effects of extrusion parameters such as temperature and extrusion ratio on the corrosion rate are discussed below.

6.1 Effect of extrusion ratio and temperature on biodegradability

The nature of the effect of extrusion on the corrosion properties is governed by the microstructure of the extruded alloy, which is a function of the extrusion parameters, such as strain rate, temperature, and velocity.

6.1.1 Effect of extrusion temperature

In order to investigate the effect of extrusion temperature on corrosion resistance of alloy, other extrusion parameters must be kept constant. BAEK et al [99] investigated the corrosion performance of Mg−8Sn−1Zn−1Al alloy in the 0.6 mol/L NaCl solution after extrusion at 180 and 280 °C (LT-E and HT-E samples, respectively) and a constant ratio of 25:1. The grain sizes of LT-E and HT-E samples were 2.9 and 4 μm, respectively. The secondary phase in the alloy, Al_5Fe_2 is highly cathodic to the alloy matrix; in fact its potential difference varies with the matrix of the alloy with respect to different extrusion temperatures, i.e., 630 and 950 mV for LT-E and HT-E respectively. As a result of this difference, within 2 h of immersion test, much larger cavities developed on the surface of HT-E sample compared to the LT-E sample, and the amount of corrosion products on the surface of HT-E sample is greater. The corrosion rates of LT-E and HT-E alloys in the immersion test after 72 h were 27.5 and 246.7 mm/a, respectively. According to Fig. 14, the alloy extruded at 280 °C has a much greater cathodic current density compared to the other sample ((−5.67±0.48) mA/cm^2 for the alloy extruded at 280 °C and (−0.62±0.033) mA/cm^2 for the alloy extruded at 180 °C at a potential of −1.8 V (vs SCE)), which indicates the high rate of cathodic reactions in this sample.

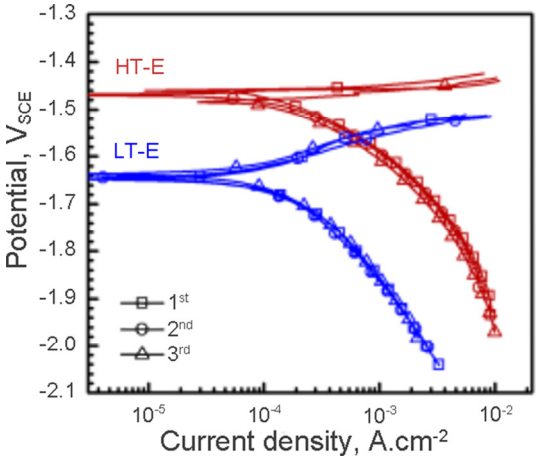

Fig. 14 Potentiodynamic polarization curves of Mg−8Sn−1Zn−1Al alloy extruded at 280 °C (HT-E) and (180 °C) LT-E in 0.6 mol/L NaCl solution [99]

MOHAMMADI and JAFARI [100] also studied the effect of extrusion temperature (300, 330 and 370 °C) on the biodegradability of Mg−5Zn−1Y−(0, 0.1, 0.5, 1 wt.%)Ca alloys. According to this study, with increasing extrusion temperature, grain size (d_G) of Mg−5Zn−1Y−(0, 1 wt.%)Ca alloys has increased (due to the growth of DRXed grains), while grain size of Mg−5Zn−1Y−(0.1, 0.5 wt.%)Ca alloys reduced, which is related to the higher start temperature of DRX (Table 6). They reported that, with increasing the density of grain boundary in alloys, the corrosion rate of both immersion and electrochemical (P_i) tests increased.

BEN-HAROUSH et al [101] surveyed the corrosion properties of AZ80 alloys after extrusion at temperatures of 250 °C (ET250 sample), 300 °C (ET300 sample) and 350 °C (ET350 sample) at the velocity of 0.12 m/min and ratio of 100%. For corrosion test, the alloys were immersed in a solution containing 3.5% NaCl and saturated

Table 6 Grain size and electrochemical corrosion parameters of as-cast and extruded Mg−5Zn−1Y−xCa alloys [100]

Alloy	300 °C		330 °C		370 °C	
	d_G/μm	P_i/(mm·a^{-1})	d_G/μm	P_i/(mm·a^{-1})	d_G/μm	P_i/(mm·a^{-1})
Mg−5Zn−1Y	13.6	1.78 ± 0.06	22.4	1.71 ± 0.06	31.6	1.69 ± 0.07
Mg−5Zn−1Y−0.1Ca	30.4	1.42 ± 0.06	18.1	1.52 ± 0.06	10.8	2.24 ± 0.06
Mg−5Zn−1Y−0.5Ca	60.2	1.11 ± 0.05	20.1	2.16 ± 0.09	13.8	2.27 ± 0.07
Mg−5Zn−1Y−1Ca	9.9	1.95 ± 0.07	11.4	1.88 ± 0.08	13.6	1.85 ± 0.07

$Mg(OH)_2$, which has a pH of 10.5. As-cast alloy microstructures consisted of three phases, matrix α, secondary phase β ($Mg_{17}Al_{12}$), and an intermetallic phase (Al_8Mn_5). Extrusion caused the arrangement of β phase as cluster with tiny debris in the longitudinal direction of extruded sample (with red arrows in Figs. 15(c, d)). The grain size of the extruded alloy has increased with the extrusion temperature. In other words, by increasing the strain and decreasing the temperature (i.e., increasing the Zener−Holman parameter), the grain size reduced (Table 7). Also, dislocation density in the microstructure of the alloy increased with the extrusion temperature; however, after the hot extrusion there was no twinning in the structure.

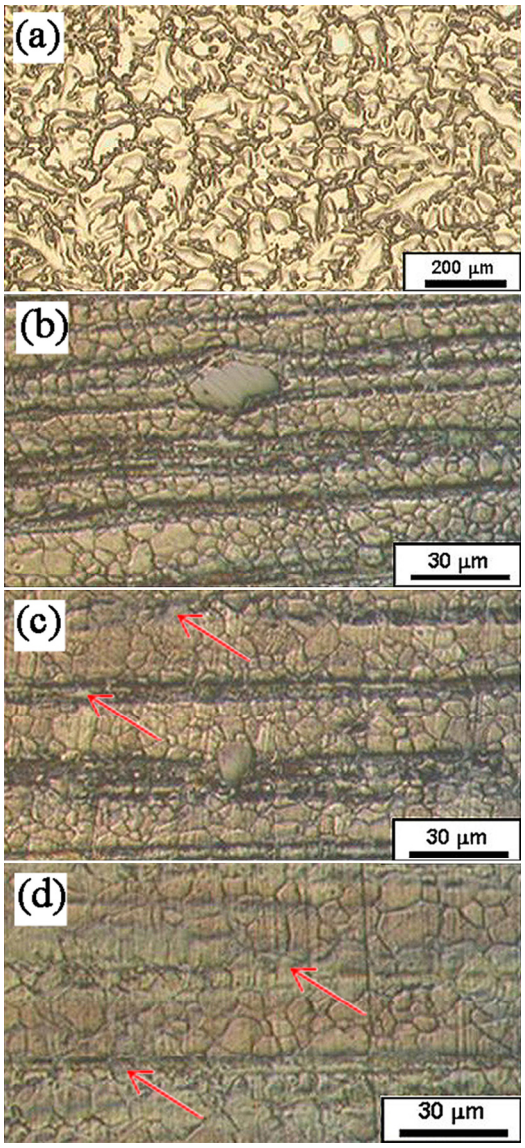

Fig. 15 Microstructure of as-cast and extruded AZ80 alloys at different extrusion temperatures: (a) As-cast; (b) 250 °C; (c) 300 °C; (d) 350 °C [101]

Table 7 Average grain size and corrosion rate of AZ80 alloys before and after extrusion [101]

Sample	Extrusion temperature/°C	Average grain size/μm	Corrosion rate/mpy
ET250	250	4.62	300
ET300	300	5.93	420
ET350	350	7.11	400

The ET250 sample exhibited higher corrosion resistance than other samples in both the electrochemical impedance spectroscopy test and the immersion test (Table 7), which is due to the low dislocation density and the finer grain size of this extruded alloy. In another study [102], it was found that in a constant extrusion ratio, the final grain size and the volume fraction of precipitates in the alloy matrix increase with increasing the extrusion temperature (Table 8).

Corrosion current density of Mg–10Gd–2Y–0.5Zr alloy rises with increasing extrusion temperature as well (Table 8 and Fig. 16). As a result of increasing the extrusion temperature and increasing the precipitates in the alloy matrix, the extent of pitting also increased. However, the corrosion mechanism of all samples was same and

Table 8 Average grain size and corrosion rate of extruded Mg−10Gd−2Y−0.5Zr alloy in 5% NaCl solution [102]

Extrusion temperature/°C	Average grain size/μm	J_{corr}/(μA·cm^{-2})
400	9.3	22
450	10.8	25
500	11.2	42

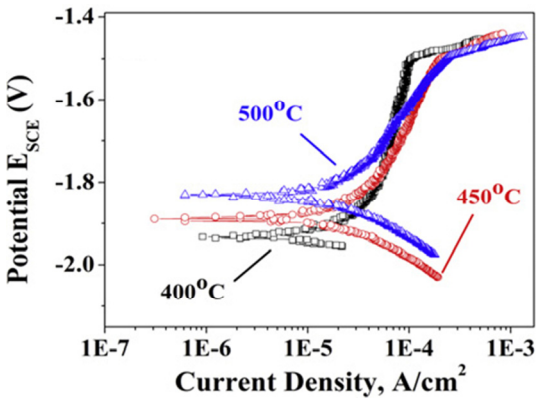

Fig. 16 Potentiodynamic polarization curves of Mg−10Gd−2Y−0.5Zr alloy extruded at different temperatures [102]

the sample extruded at 400 °C had the highest corrosion resistance.

LI et al [103] confirmed that the increase in the corrosion rate of the Mg–2Nd–0.2Zn alloy is due to the increase of extrusion temperature (Table 9). The sample extruded at 390 °C (E1) showed passive behavior and greater corrosion resistance (Fig. 17), and the predominant corrosion mechanism in this sample was the uniform corrosion, while the sample extruded at 500 °C (E2) suffered pitting, and higher corrosion rate in the immersion test (Fig. 18). They also reported that the ultimate tensile strength (UTS) of the E1 and E2 samples was almost the same. But the yield strength (YS) of the E1 sample was higher than that of the E2 sample, while the elongation of the E1 sample was lower than that of the E2 sample (Table 9). Compared with the E2 sample, the finer grain size in the E1 sample leads to an increase in the YS according to the Hall−Patch relationship.

JAFARI et al [54] reported that although the increase in extrusion temperature causes a more homogenous microstructure of ZX10 alloy, corrosion behavior of the alloy is not affected and polarization curves of the samples remain unchanged. They discovered that the alloy extruded at lower temperature offered superior tensile and fatigue properties due to the grain-boundary strengthening mechanism.

The simultaneous effect of temperature and extrusion ratio on the microstructure, mechanical properties, and biodegradability of Mg−3Nd−0.2Zn−0.4Zr alloy was studied by ZHANG et al [26,27]. According to their investigation, corrosion resistance decreased with increasing temperature and extrusion ratio. At first, as-cast alloy was solution treated (T4) at 540 °C for 10 h and then extruded at 250 °C (E250), 350 °C (E350) and 450 °C (E450) with the extrusion ratio of 25:1. After solution treatment, a uniform microstructure without eutectic phases was obtained. However, after the aging process, followed by extrusion, the secondary phase was observed in the structure. DRX caused by the extrusion led to reduction in grain size. The final grain size increased with the extrusion temperature. Investigation of the fracture surface indicates a brittle fracture in the case of the solution-treated sample and a completely ductile fracture surface in the extruded samples. The results of mechanical properties represent that the YS decreases with the rise of extrusion temperature as a result of grain coarsening at higher temperatures (Table 10). Also, the corrosion rate of each sample is given in Table 10.

Table 9 Grain size and electrochemical corrosion parameters of Mg−2Nd−0.2Zn alloy extruded at 390 °C (E1) and 500 °C (E2) [103]

Sample	Average grain size/μm	J_{corr}/(μA·cm^{-2})	φ_{corr}/V	R_p/kΩ	Corrosion rate/(mm·a^{-1})	YS/MPa	UTS/MPa	Elongation/%
E1	7.2−7.8	3.5	−1.56	7.45	0.19	119	200	33
E2	12.2−12.4	10.7	−1.61	1.59	0.58	84	194	37

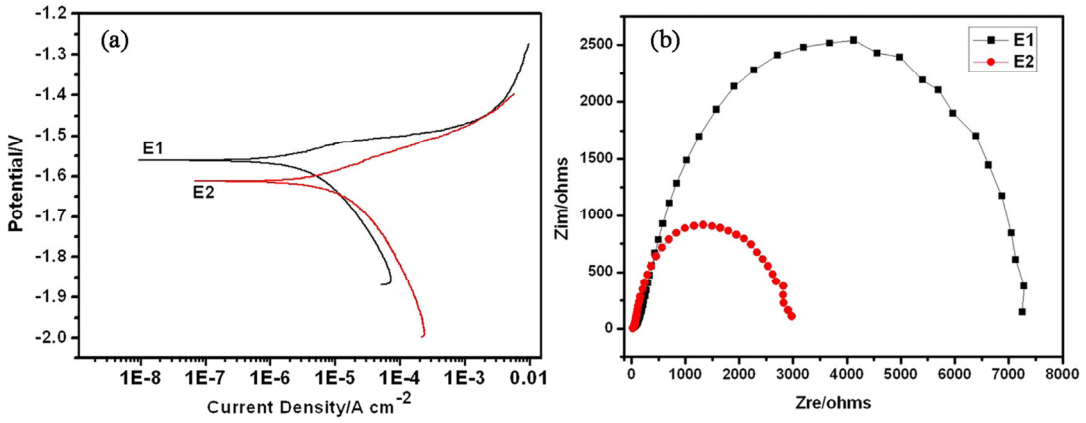

Fig. 17 Polarization curves (a) and Nyquist plots (b) of Mg–2Nd–0.2Zn alloy extruded at different temperatures shown in Table 9, and tested in SBF [103]

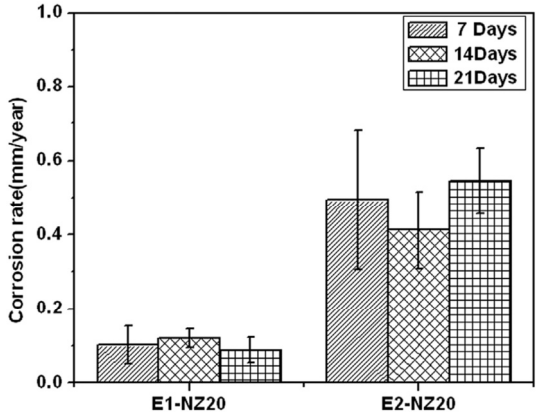

Fig. 18 Corrosion rates of extruded Mg–2Nd–0.2Zn alloy during immersion in Hanks solution [103]

Table 10 Corrosion rates of Mg−3Nd−0.2Zn−0.4Zr alloy extruded at different temperatures [26]

Sample	Extrusion temperature/ °C	Corrosion rate/ mpy	YS/ MPa	UTS/ MPa	Elongation/ %
T4	−	0.37	90±7	194±3	12±0.8
E250	250	0.22	162±1	234±1	26±0.7
E350	350	0.26	145±2	229±3	25±1.5
E450	450	0.28	124±2	226±2	22±0.3

As shown in Fig. 19, with increasing the extrusion temperature, the amount of released hydrogen gas in the SBF solution increased. Extruded samples represent the lowest corrosion rates during the immersion test. On the surface of the corroded samples, the hydroxyapatite structure was observed. By increasing the immersion time, the surface film became more compact. However, with the penetration of the Cl^- ion, the film was gradually disrupted. Also, samples are corroded by the same mechanisms and only differ in the corrosion rate.

6.1.2 Effect of extrusion ratio

Another study by ZHANG et al [27] was performed on the Mg−3Nd−0.2Zn−0.4Zr alloy at the constant extrusion temperatures of 320 °C and the extrusion ratios of 8:1 (R8) and 25:1 (R25). Also, before the extrusion, the alloy was solution treated (T4) at 540 °C for 10 h. Solution treatment led to the dissolution of all alloying elements; however, some Zr remained at/near the grain boundaries. For the sample extruded at the lower ratio, elongated grains were observed initially which lengthened along the longitudinal direction of extrusion. However, these grains disappeared upon increasing the extrusion ratio (that caused dynamic recrystallization).

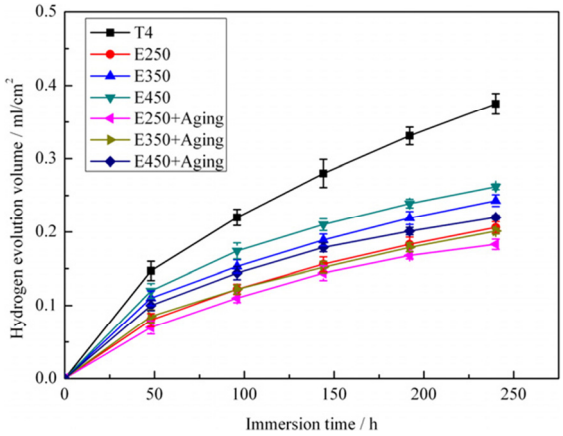

Fig. 19 Hydrogen evolution rates of Mg−Nd−Zn−Zr alloys before and after extrusion at different temperatures in SBF [26]

On the other hand, increasing the extrusion ratio leads to the increase of the average grain size and the grains become more homogeneous. Strain of the structure increases with increasing extrusion ratio, and as a result, the starting temperature of recrystallization decreases. Therefore, the deformation energy increases and the internal temperature of the alloy rises during the process. As a result, when extrusion ratio is large, complete DRX occurred. However, increasing the extrusion ratio causes the reduction of the corrosion resistance (Table 11). Accordingly, R8 alloy has the lowest amount of released hydrogen gas after 250 h immersion and also the lowest corrosion rate (Fig. 20 and Table 11). In general, by reducing the grain size, the corrosion rate decreases. The finer the grains and the precipitate (R8) are, the higher the strength is, but the lower the elongation is (Table 11).

Table 11 Average grain size and corrosion rates of Mg−3Nd−0.2Zn−0.4Zr alloy before and after extrusion at different extrusion ratios [27]

Sample	Average grain size/ μm	Corrosion rate/ ($mm \cdot a^{-1}$)	YS/ MPa	UTS/ MPa	Elongation/ %
T4	45	0.37	90±7	194±3	12.0±0.8
R8	2	0.11	308±6	312±2	12.2±0.6
R25	5	0.23	156±1	233±4	25.9±0.8

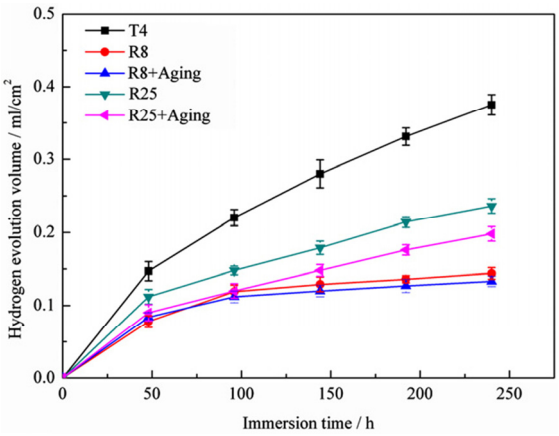

Fig. 20 Hydrogen evolution rates of Mg−Nd−Zn−Zr alloy before and after extrusion at different extrusion ratios and tested in SBF [27]

In another study, Mg−2Zn−0.2Mn alloy was extruded at a constant temperature of 330 °C and variable extrusion ratios of 12:1 (ER12), 25:1 (ER25), and 33:1 (ER33), at a velocity of 3 mm/s [104]. As the extrusion ratio increases, first, the grain size decreases and then increases. ER25 produced the smallest average grain size. On the other hand, the corrosion current density decreases with increasing extrusion ratio, and the corrosion potential becomes nobler. Nevertheless, the results of the hydrogen gas release tests in the Hanks solution was reported to have a different trend, and the ER25 sample had the least amount of released hydrogen gas (Table 12). Increasing the extrusion ratio increased the percentage of DRX; however, in larger extrusion ratios, secondary recrystallization occurred and grain size increased. Accordingly, corrosion resistance, UTS, and elongation increased with the increase of the extrusion ratio from 0 to 25:1 and then decreased sharply with a further increasing of extrusion ratio to 33:1 (Table 12).

Table 12 Electrochemical corrosion parameters and hydrogen evolution rates of as-cast and extruded Mg−2Zn−0.2Mn alloy [104]

Sample	J_{corr}/ ($\mu A \cdot cm^{-2}$)	φ_{corr}/ V	Hydrogen evolution rate/ ($mL \cdot cm^{-2} \cdot d^{-1}$)	UTS/ MPa	Elongation/ %
As-cast	31.6	−1.571	0.4	125.5	15
ER12	0.63	−1.517	0.081	230	14.1
ER25	0.62	−1.498	0.022	316	33
ER33	0.61	−1.492	0.044	160	12.8

XU et al [105] reported that increasing the extrusion ratio results in the improvement of the corrosion resistance of Mg−2.5Y alloy (Table 13). This alloy was extruded at a constant temperature of 260 °C and extrusion ratios of 5:1 and 20:1. A homogeneous microstructure, with broken and diffused secondary phases in the matrix of alloy, was observed in this alloy after the extrusion.

Table 13 Electrochemical corrosion parameters of extruded Mg−2.5Y alloy [105]

Extrusion ratio	Lateral direction		Longitudinal direction	
	J_{corr}/ ($\mu A \cdot cm^{-2}$)	φ_{corr}/ V	J_{corr}/ ($mA \cdot cm^{-2}$)	φ_{corr}/ V
5:1	475.46	−1.534	384.78	−1.486
20:1	447.38	−1.487	354.93	−1.432

Increasing the extrusion ratio led to the enhancement of the deformation rate and grain recrystallization resulted in a fine-grained alloy. At low extrusion ratio, the heterogeneity of the microstructure was evident (Fig. 21). By increasing the extrusion ratio the corrosion potential becomes nobler and corrosion current density of the alloy decreases (Table 13). Also, based on the result of the potantiodynamic polarization tests, the corrosion current density of the samples in the longitudinal direction of extrusion is greater than that in the radial direction of extrusion. Results of the immersion test in 3.5% NaCl solution were consistent with those of the polarization test and the sample extruded at higher extrusion ratios and in the longitudinal direction had the lowest corrosion rate (Fig. 22).

In another study, AZ31 alloy was extruded at 723 K with the extrusion ratios of 11:1, 25:1, and 44.4:1, and the extrusion rate of 0.1 mm/s [106]. Corrosion test of the alloy was performed by immersion in 4% NaCl solution for 3 d at pH 7 and 10. According to Table 14, by increasing the extrusion ratio, the grain size was reduced and a more homogeneous structure was obtained. Due to the high temperature of the extrusion and the low stacking fault energy (SFE) of magnesium, DRX was observed in all extruded samples. In the sample extruded at extrusion ratio of 11:1, large and small heterogeneous grains were visible, but with increasing extrusion ratio (increasing strain and strain rate, and finally density of dislocations), the grains became axial. The secondary phases did not

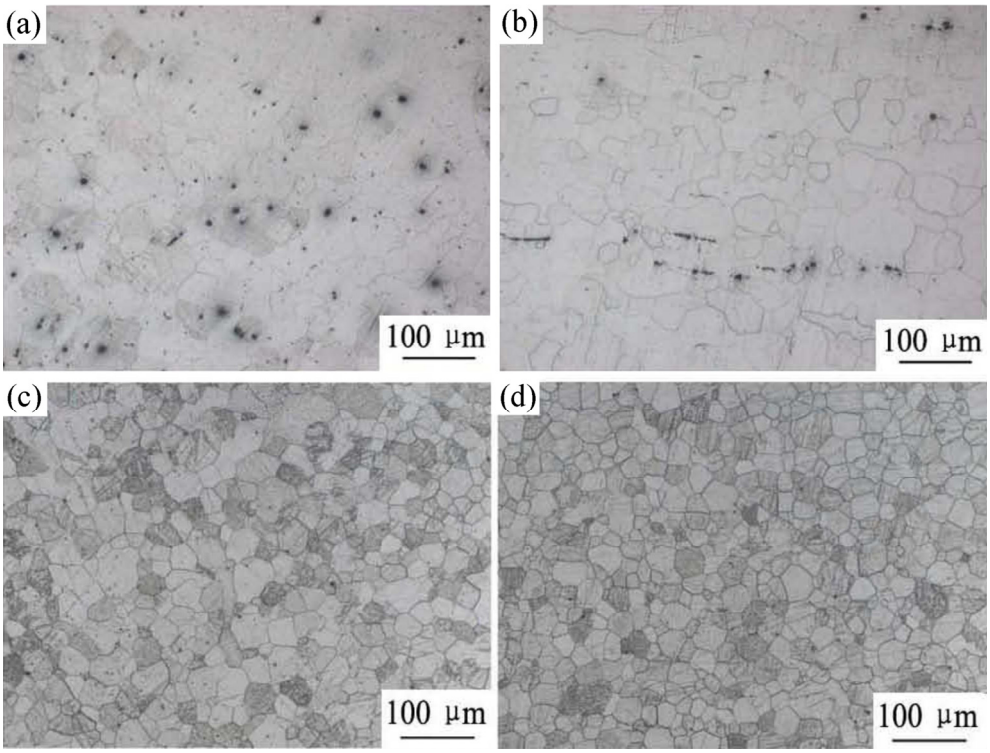

Fig. 21 Lateral microstructure (a, c) and longitudinal microstructure (b, d) of Mg−2.5Y alloy extruded at extrusion ratios of 5:1 (a, b) and 20:1 (c, d) [105]

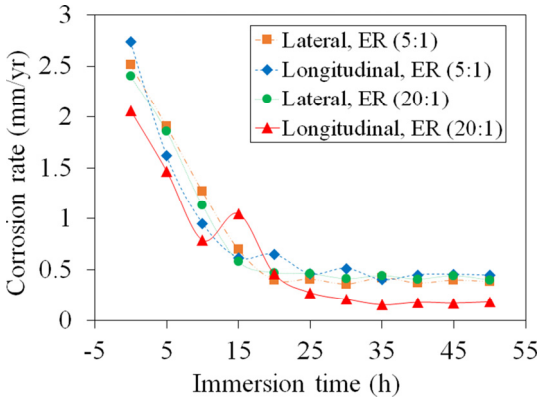

Fig. 22 Corrosion rates of extruded Mg−2.5Y alloy during immersion time in 3.5% NaCl solution [105]

precipitate in any of the samples. Tensile and yield strengths improved with increasing extrusion ratio. Fractography suggested all samples to have undergone a mix of ductile and brittle fracture, and micro-cracks were evident on the surface of the samples. However, the sample extruded with a ratio of 25:1 had a wider ductile fracture. The sample extruded with a ratio of 44.4:1 had a higher amount of micro-cracks, which can be due to the high residual stress in the sample due to the extrusion. As the extrusion ratio increased, the corrosion rate decreased (Table 14). Nonetheless, the corrosion rate of the samples in solution with pH=10 is lower, presumably because of the passivizing influence of the alkaline constituent of the test solution. All the corroded surfaces had features of localized corrosion and pitting.

SHIRI and JAFARI [29] conducted a comprehensive study on the simultaneous effect of both extrusion parameters (temperature and ratio) on the corrosion resistance of the binary magnesium−zinc alloy (Mg−4.5Zn). After the solid solution treatment at 400 °C for 30 h, the alloy was extruded at three temperatures and three different ratios (Table 15). Then, its corrosion performance in SBF solution was studied using polarization and immersion methods. Extrusion at lower temperatures and higher ratios led to the increase of the internal energy of the alloy. As a result, DRX is accelerated and axial grains are formed in the alloy with certain extrusion treatment (R18-T300, R12-T300, R6-T300 and R18-T350). It was found that as the temperature of the mechanical work increases, the starting temperature of the DRX also increases, leading to a decrease in rate and an increase in the internal energy of the samples extruded at higher temperatures. As a result, heterogeneous grain growth occurred in these

Table 14 Dependence of average grain size and corrosion rates of AZ31 alloy on extrusion ratio [106]

Extrusion ratio	Average grain size/μm	Corrosion rate in 4% NaCl solution with pH of 10 ($g·mm^{-2}·d^{-1}$)	Corrosion rate in 4% NaCl solution with pH of 7 ($g·mm^{-2}·d^{-1}$)	YS/ MPa	UTS/ MPa	Elongation/ %
11:1	27	8.78×10^{-6}	11.25×10^{-6}	223	305	15
25:1	10.5	7.65×10^{-6}	9.63×10^{-6}	192	295	15.4
44.4:1	6.3	5.41×10^{-6}	7.44×10^{-6}	155	271	10.8

Table 15 Average grain size, electrochemical corrosion parameters, and corrosion rates of Mg−4.5Zn alloy soaked in SBF [29]

Sample	Extrusion temperature/°C	Extrusion ratio	Average grain size/μm	Electrochemical parameter		Immersion test result
				φ_{corr}(vs SCE)/mV	J_{corr}/(μA·cm^{-2})	CR/(mm·a^{-1})
R18-T300	300	18:1	18.2±1.2	−1606±10	39±2	0.882
R12-T300	300	12:1	19.1±1.8	−1602±11	48±2	0.988
R6-T300	300	6:1	20.1±1.5	−1601±10	51±2	0.995
R18-T350	350	18:1	19.5±1.5	−1606±12	41±1	1.058
R12-T350	350	12:1	19.5±1.6	−1611±12	49±2	1.281
R6-T350	350	6:1	20.9±1.7	−1698±16	69±3	1.257
R18-T400	400	18:1	20.6±1.4	−1681±16	66±3	1.164
R12-T400	400	12:1	25.1±1.6	−1701±17	74±5	1.367
R6-T400	400	6:1	27.1±1.8	−1680±15	75±4	1.415

samples, and lots of coarse grains were observed in the vicinity of the fine grains (as shown for R12-T350, R6-T350, R18-T400, R12-T400, and R6-T400 specimens in Fig. 23). Since the number of initial DRX nuclei depends on the amount of deformation, so with decreasing deformation or extrusion ratio, the number of DRX grains in the microstructure decreased and therefore elongated, and relatively large grains were observed in some specimens extruded at lower ratios, such as R6-T350 and R6-T400. Generally, with increasing extrusion ratio and decreasing temperature of this process, the grain size decreased, and the sample extruded at 300 °C and ratio of 18 had the lowest average grain size (about 18.2 μm), and the sample extruded at 400 °C and ratio of 6 had the highest average grain size (approximately 27.1 μm).

The results of immersion corrosion tests confirmed the potantiodynamic polarization test results, indicating that with increasing extrusion ratio and decreasing extrusion temperature, the corrosion rate of the alloy decreased. The sample with the lowest average grain size had the lowest corrosion rate, as suggested both in immersion and polarization tests. Presumably, the presence of heterogeneous microstructure also caused the formation of internal galvanic cells.

In samples with greater grain size differences in the microstructure, higher corrosion rates have been reported. On the other hand, the smaller average size as well as the homogeneity of the microstructure increased the corrosion resistance of the alloy (extruded at 300 °C). Finally, SHIRI and JAFARI [29] provided a relationship between grain size (d) and the amount of the corrosion current density of the polarization:

$$J_{corr}=A+Bd^{-0.5} \quad (4)$$

where A is the constant depending on the electrolyte solution, and B is the constant depending on the microstructure of the alloy. The plot obtained from this equation confirms the inverse relationship between the average grain size and the corrosion current density of the extruded alloy (Fig. 24).

6.2 Overall roles of extrusion ratio and temperature

Extrusion parameters impact the bio-degradation performance of magnesium alloys due to the three main factors, including mean final grain size, precipitations, and texture. The higher the

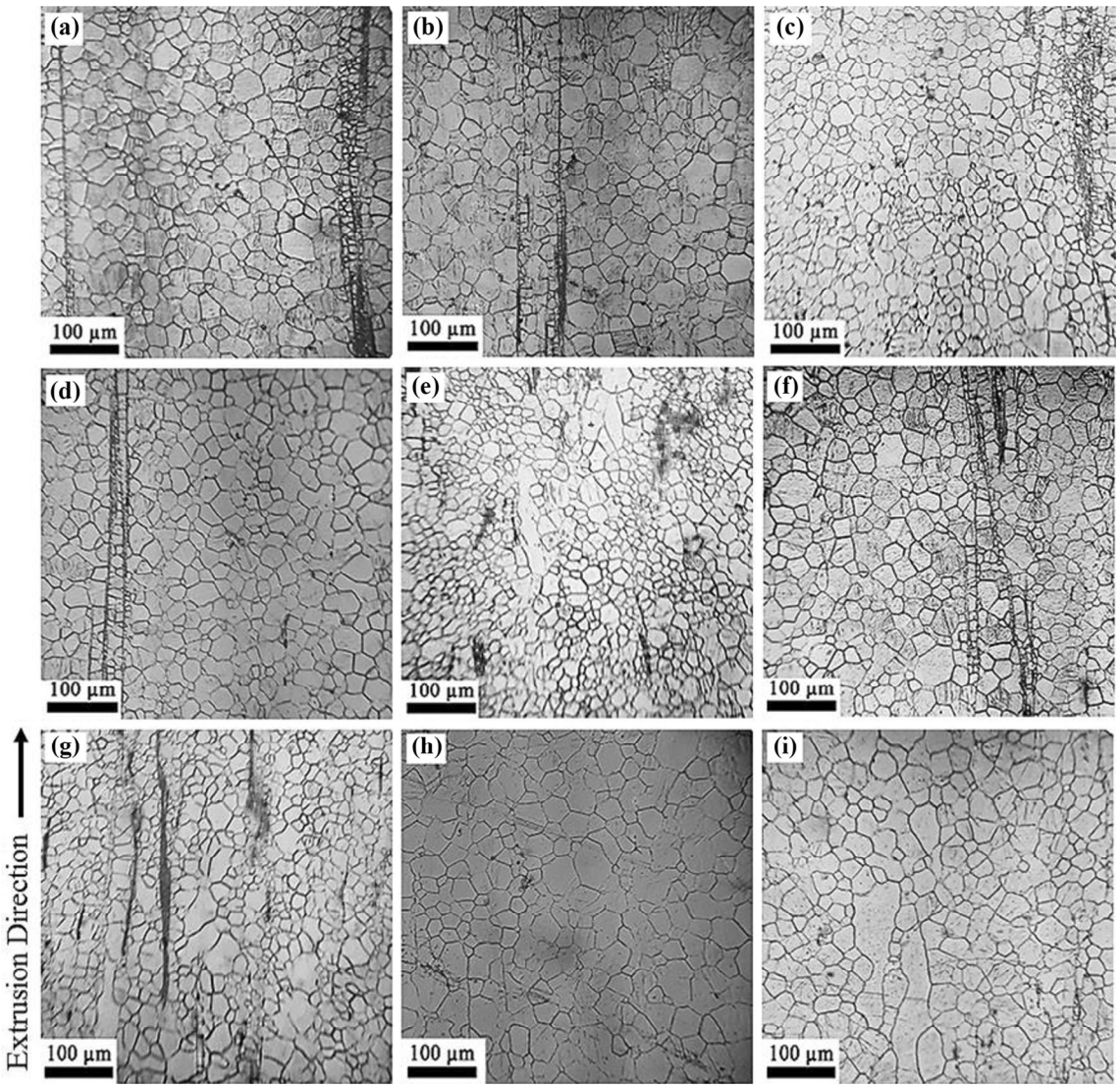

Fig. 23 Microstructures of extruded Mg−4.5Zn alloy: (a) R18-T300; (b) R12-T300; (c) R6-T300; (d) R18-T350; (e) R12-T350; (f) R6-T350; (g) R18-T400; (h) R12-T400; (i) R6-T400 [29]

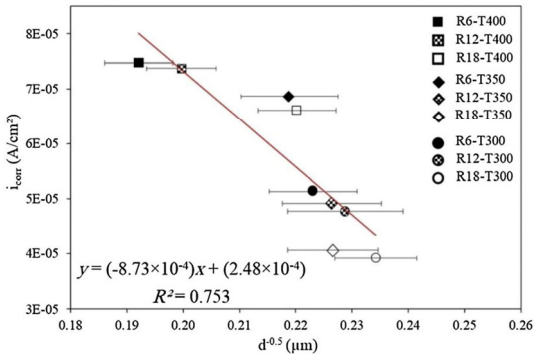

Fig. 24 Relationship between average grain size and corrosion current density of extruded Mg−4.5Zn alloy [29]

extrusion ratio, or the lower the extrusion temperature, the finer and the more axial final grains. This is attributed to the rise in DRX volume due to a higher strain rate at a lower temperature in the semi-hot or hot deformation work. Temperature (T) and strain rate ($\dot{\varepsilon}$) of the hot-mechanical working can be defined by the Zener−Holman parameter ($Z=\dot{\varepsilon}\cdot\exp[Q/(RT)]$). This parameter is in inverse relationship with grain size [29]. The growth of recrystallized grain is enhanced by the rise of extrusion temperature [26]. Also, the decrease in extrusion ratio culminates in heterogeneous microstructure, where there are DRXed grains that are adjacent to none-DRXed grains elongated in a parallel line with the extrusion direction [105]. One of the main strategies to produce magnesium alloy with a lower corrosion rate is the improvement in the protectiveness of the

corrosion product film [107]. As grain boundaries are active areas and have lower activation energy, electron activities and the atom diffusion rate are raised in it, which means that the nucleation of the $Mg(OH)_2$ layer is intensified at the earlier time of immersion [108]. In terms of corrosion resistance, it is easier for finer grains of magnesium alloy on the surface to accommodate stresses developed during formation of MgO and $Mg(OH)_2$. Although the grain boundaries promote corrosion at first, they are conducive to the passivation process and reduce the corrosion rate of the alloy in the next stage [105].

$Mg(OH)_2$ layer blankets the stable MgO layer which is primarily covered the surfaces of immersed alloy. These layers present a good corrosion resistance in C-SBF, and their immunity in the solution is attributed to strong bonds between them due to a moderately low mismatch factor they have [108,109]. In addition to grain refining, lowering the galvanic corrosion of immersed magnesium alloys is another approach for reducing its corrosion rate. The presence of homogenous axial grains lowers the microgalvanic corrosion [24,29,108]. Corroded grain boundaries at the earlier period of immersion are fully covered with the robust, continuous and adhesive $Mg(OH)_2$ layer, which restricts the developing microgalvanic couples between the interior and exterior grains [110]. Therefore, the higher the grain boundaries volume, the greater the amount of the $Mg(OH)_2$ layer, and conclusively the lower the corrosion rate.

With the alignment of basal plane in parallel to the extrusion direction, magnesium alloys provide better corrosion resistance especially when the surface parallel to the extrusion direction is immersed in the solution. This more-closely packed plane has the greatest atomic density among the hcp crystallographic planes, which causes lower surface energy. The higher intensity of such plane leads to restriction of corrosion rate [95,111].

The rise of temperature in hot mechanical works results in a reduction of basal texture intensity due to the rise of both atomic self-diffusion rates and activity of various slip systems and formation of dynamic precipitates. Accordingly, the activity of the none-basal slip system is greater at a higher temperature compared to that of a lower temperature; and also the precipitates can lead to dislocation pile-up. These areas act as the preferential areas for nucleation of new grains with random orientations culminating in basal texture weakening [92,112]. Meanwhile, the higher extrusion ratio breeds greater shear force acting on the grains in AZ31 and increases the deformation degree of grains, which eventually gives rise to the formation of the more basal plane in the parallel direction to extrusion direction [113].

The volume fraction and size of precipitates increase with the rise of extrusion temperature. This brings about a microgalvanic effect, leading to a higher corrosion rate [102]. CAO et al [114] represented that corrosion of the magnesium matrix was accelerated, where there are precipitated particles at the interior of the grains, through the microgalvanic impact of the impurity precipitates. Also, as stated by ATRENS [115], ultra highly purified magnesium alloys represent corrosion rates significantly better than the best available current magnesium alloys that all have corrosion rates equal to or higher than that of highly purified magnesium. Meanwhile, precipitating along the grain boundaries encourages pitting or easily deepening the depth of pits [102].

On the other hand, very tiny secondary particles disperse in both grain boundaries and the interior of the grains in the Mg-rare earth alloys upon extrusion at low temperature or high ratio. They have a slightly more positive corrosion potential than the magnesium matrix and reduce the galvanic effect [103,105]. To add more, magnesium alloyed with rare earth elements such as Nd, produces a second phase with the capability of high activity of galvanic corrosion. The second phase ($Mg_{12}Nd$) provides corrosion potential which is only a little more positive than that of pure magnesium. The alloy, which has a DRXed microstructure with finer grains as well as uniformly distributed corrosion barrier second phases, exhibits some passivity upon the immersion test [27].

Increasing the extrusion ratio crushes eutectic phases of the as-cast magnesium alloy and spreads them uniformly in the extruded micro-structure [105]. Not just do the phases act as nuclei for new grains, but they hinder the movement of grain boundaries and postpone the grain growth, resulting in the formation of finer and equiaxed grains in the extruded microstructure.

In terms of the extrusion temperature,

precipitation of nano-scale second phases has close potential to magnesium matrix, and uniformly dispersion of these particles due to extruding at lower extrusion temperature makes the serious localized corrosion difficult to happen and hinders the spread of the corrosion. Extrusion at the lower temperature results in the extreme crushing of the particles, which serves as the crystal nucleus and blocks the grain boundaries movement as well [103].

Additionally, the nobility of the second phases impacts the corrosion rate [99,101]. For instance, as reported by BAEK et al [99], the lower the extrusion temperature, the nobler the second phase (Al_5Fe_2) on the extruded magnesium alloy. The nobility of the particles lowers the cathodic regions in the magnesium matrix, resulting in retarded microgalvanic corrosion between the matrix and the second phase. The rise of Mn content on the second phase whose size and volume fraction are relatively smaller at the lower extrusion temperature leads to the improvement of the second phase nobility [99].

7 Summary and conclusions

Biodegradable magnesium alloys possess attractive characteristics for a potential material for biodegradable implants. Using different processing methods, the corrosion resistance of these alloys can be enhanced to the appropriate range, so that before the complete degradation of the implant, the damaged body tissue regains its strength and performance. There are methods that, in addition to improving biodegradability, improve the strength and flexibility of magnesium alloys. Methods such as alloying with biocompatible elements, solution treatment and hot extrusion enhance the corrosion resistance and mechanical performance of these alloys. The microstructure of the alloy (including size and shape of grains, amount, shape and size of precipitates, amount of twinning and dislocations, texture, etc.) can be greatly improved after the hot extrusion process that leads to the increase of corrosion resistance and mechanical strength of the alloy. The outcomes of this review are summarized as follows.

(1) After hot extrusion process, the average final grain size of magnesium alloy decreases. As the grain size decreases, formation of surface film of MgO is facilitated which is more compatible with the metal surface; MgO also facilitates formation of $Mg(OH)_2$ passive layer. As a result, the alloy surface provides greater resistance to attack by Cl^- ions. A fine-grained alloy shows superior corrosion resistance. Also, the physical decomposition and dispersion of the precipitates during extrusion have a positive effect on improving the corrosion resistance.

(2) At high strain rates (high extrusion ratio) and severe plastic deformation that is accompanied by low deformation temperature, the amount of dislocations, twinning and heterogeneity increase in the structure and residual stress also rises in the alloy. As a result, the internal energy of the structure increases and dynamic recrystallization (DRX) is activated at lower temperatures. Therefore, alloy with such treatment contains axial and more homogeneous grains.

(3) Extrusion in lower temperature and/or higher ratio causes basal texture strengthening in most magnesium alloys; and due to the low surface energy of the {0001} plates, the basal texture creates better corrosion resistance.

(4) Generally, at a constant extrusion ratio, by increasing the temperature of extrusion and delaying DRX, the grains growth is heterogeneous and the grains are heterogeneously arranged in the final structure of the alloy, and the average final grain size of magnesium alloy increases. As the temperature of the extrusion increases and heterogeneity of the final microstructure rises, the corrosion rate of alloy increases.

(5) At the constant temperature, with increasing extrusion ratio, the recrystallization temperature in magnesium alloy decreases and the final grain size decreases. However, variation of the extrusion ratio has very little effect on the grain size of DRX. At low extrusion ratios and due to delay in the beginning of DRX, the number of the elongated and unDRXed grains is high. By increasing the extrusion ratio and decreasing the grain size, the volume fraction of the precipitates decreases, but they become larger. The presence of a large volume of different grain sizes reduces corrosion resistance. As the extrusion ratio is enhanced (until the grain growth does not occur), because of the increase in the percentage of DRXed grains, the microstructure becomes more homogeneous, and the volume of the

different grain sizes decreases and the corrosion resistance increases.

References

[1] WILLIAMS D F. Definitions in biomaterials [M]. Amsterdam: Elsevier, 1987.

[2] PARK J B, LAKES R S. Biomaterials−An introduction [M]. 2nd ed. New York: Plenum Press, 1992.

[3] Structural hierarchy in materials & biology [R]. USA: Massachusetts Institute of Technology (MIT), 2006, http://ocw.mit.edu/index.htm.

[4] JIN Wei-hong, CHU P K. Orthopedic implants [C]// Encyclopedia of Biomedical Engineering. Amsterdam: Elsevier, 2019: 425−439.

[5] CHEN Q Z, THOUAS G A. Metallic implant biomaterials [J]. Materials Science and Engineering: R, 2015, 87: 1−57.

[6] HAYNES D R, ROGERS S D, HAY S, PEARCY M J, HOWIE D W. The differences in toxicity and release of bone-resorbing mediators induced by titanium and cobalt−chromium-alloy wear particles [J]. Emerging Infectious Diseases, 1993, 75: 825−834.

[7] WANG J C, YU W D, SANDHU H S, BETTS F, BHUTA S, DELAMARTER R B. Metal debris from titanium spinal implants [J]. Spine, 1999, 24: 899−903.

[8] RATNER B D, HOFFMAN A S, SCHOEN F J, LEMONS J E. Biomaterials science: An evolving, multidisciplinary endeavor [C]//Biomaterials Science. Amsterdam: Elsevier, 2013: 1−20.

[9] JAFARI H, HESSAM H, SHAHRI S M G, ASSADIAN M, HAMTAIE SHAIRAZIFARD S H P, IDRIS M H. Characterizing sintered nano-hydroxyapatite sol−gel coating deposited on a biomedical Ti−Zr−Nb alloy [J]. Journal of Materials Engineering and Performance, 2016, 25: 901−909.

[10] PERSAUD-SHARMA D, MCGORON A. Biodegradable magnesium alloys: A review of material development and applications [J]. Journal of Biomimetics, Biomaterials and Tissue Engineering, 2012, 12: 25−39.

[11] UPPAL G, THAKUR A, CHAUHAN A, BALA S. Magnesium based implants for functional bone tissue regeneration — A review [J]. Journal of Magnesium and Alloys, 2022, 10: 356−386.

[12] YAN Jun, CHEN Yi-gang, YUAN Qing-ling, WANG Xiao-hu, YU Song, QIU Wen-cai, WANG Zhi-gang, AI Kai-xing, ZHANG Xiao-nong, ZHANG Shao-xiang, ZHAO Chang-li, ZHENG Qi. Comparison of the effects of Mg–6Zn and Ti–3Al–2.5V alloys on TGF-β/TNF-α/VEGF/b-FGF in the healing of the intestinal tract in vivo [J]. Biomedical Materials, 2014, 9: 025011.

[13] BRAR H S, PLATT M O, SARNTINORANONT M, MARTIN P I, MANUEL M V. Magnesium as a biodegradable and bioabsorbable material for medical implants [J]. JOM, 2009, 61: 31−34.

[14] VORMANN J. Magnesium: nutrition and metabolism [J]. Molecular Aspects of Medicine, 2003, 24: 27−37.

[15] SONG Ming-shi, ZENG Rong-chang, DING Yun-fei, LI R W, EASTON M, COLE I, BIRBILIS N, CHEN Xiao-bo. Recent advances in biodegradation controls over Mg alloys for bone fracture management: A review [J]. Journal of Materials Science & Technology, 2019, 35: 535−544.

[16] STAIGER M P, PIETAK A M, HUADMAI J, DIAS G. Magnesium and its alloys as orthopedic biomaterials: A review [J]. Biomaterials, 2006, 27: 1728−1734.

[17] SONG Ying-wei, HAN En-hou, DONG Kai-hui, SHAN Da-yong, YIM Chang-dong, YOU Bong-sun. Effect of hydrogen on the corrosion behavior of the Mg−xZn alloys [J]. Journal of Magnesium and Alloys, 2014, 2: 208−213.

[18] NOVIANA D, PARAMITHA D, ULUM M F, HERMAWAN H. The effect of hydrogen gas evolution of magnesium implant on the postimplantation mortality of rats [J]. Journal of Orthopaedic Translation, 2016, 5: 9−15.

[19] IQBAL N, IQBAL S, IQBAL T, BAKHSHESHI-RAD H R, ALSAKKAF A, KAMIL A, ABDUL KADIR M R, IDRIS M H, RAGHAV H B. Zinc-doped hydroxyapatite−zeolite/ polycaprolactone composites coating on magnesium substrate for enhancing in-vitro corrosion and antibacterial performance [J]. Transactions of Nonferrous Metals Society of China, 2020, 30: 123−133.

[20] MA Ying-zhong, WANG De-xin, LI Hong-xiang, YANG Chang-lin, YUAN Fu-song, ZHANG Ji-shan. Microstructure, mechanical properties and corrosion behavior of quaternary Mg−1Zn−0.2Ca−xAg alloy wires applied as degradable anastomotic nails [J]. Transactions of Nonferrous Metals Society of China, 2021, 31: 111−124.

[21] BAIRAGI D, MANDAL S. A comprehensive review on biocompatible Mg-based alloys as temporary orthopaedic implants: Current status, challenges, and future prospects [J]. Journal of Magnesium and Alloys, 2022, 10: 627−669.

[22] GU Xue-nan, ZHENG Yu-feng, CHENG Yan, ZHONG Sheng-ping, XI Ting-fei. In vitro corrosion and biocompatibility of binary magnesium alloys [J]. Biomaterials, 2009, 30: 484−498.

[23] ZHANG Shao-xiang, ZHANG Xiao-nong, ZHAO Chang-li, LI Jia-nan, SONG Yang, XIE Chao-ying, TAO Hai-rong, ZHANG Yan, HE Yao-hua, JIANG Yao, BIAN Yu-jun. Research on an Mg−Zn alloy as a degradable biomaterial [J]. Acta Biomaterialia, 2010, 6: 626−640.

[24] LIU De-xue, GUO Cheng-gong, CHAI Li-qiang, SHERMAN V R, QIN Xiao-qiong, DING Yu-tian, MEYERS M A. Mechanical properties and corrosion resistance of hot extruded Mg–2.5Zn–1Ca alloy [J]. Materials Science and Engineering B, 2015, 195: 50−58.

[25] PENG Qiu-ming, LI Xue-jun, MA Ning, LIU Ri-ping, ZHANG Hong-jie. Effects of backward extrusion on mechanical and degradation properties of Mg−Zn biomaterial [J]. Journal of the Mechanical Behavior of Biomedical Materials, 2012, 10: 128−137.

[26] ZHANG Xiao-bo, YUAN Guang-yin, MAO Lin, NIU Jia-lin, FU Peng-huai, DING Wen-jiang. Effects of extrusion and heat treatment on the mechanical properties and biocorrosion behaviors of a Mg−Nd−Zn−Zr alloy [J]. Journal of the Mechanical Behavior of Biomedical Materials, 2012, 7: 77−86.

[27] ZHANG Xiao-bo, YUAN Guang-yin, NIU Jia-lin, FU Peng-huai, DING Wen-jiang. Microstructure, mechanical properties, biocorrosion behavior, and cytotoxicity of as-extruded Mg–Nd–Zn–Zr alloy with different extrusion

ratios [J]. Journal of the Mechanical Behavior of Biomedical Materials, 2012, 9: 153−162.

[28] JAFARI H, TEHRANI A H M, HEYDARI M. Effect of extrusion process on microstructure and mechanical and corrosion properties of biodegradable Mg−5Zn−1.5Y magnesium alloy [J]. International Journal of Minerals, Metallurgy and Materials, 2022, 29: 490−502.

[29] SHIRI M, JAFARI H. Effect of extrusion temperature and extrusion ratio on microstructure and biodegradation behavior of Mg−4.5Zn binary alloy [J]. JOM, 2019, 71: 4705−4714.

[30] RATNER B D, HOFFMAN A S, SCHOEN F J, LEMONS J E. Biomaterials science: An introduction to materials in medicine [M]. 2nd ed. San Diego: Academic Press, 2004.

[31] SINGH RAMAN R K, JAFARI S, HARANDI S E. Corrosion fatigue fracture of magnesium alloys in bioimplant applications: A review [J]. Engineering Fracture Mechanics, 2015, 137: 97−108.

[32] WITTE F, KAESE V, HAFERKAMP H, SWITZER E, MEYER-LINDENBERG A, WIRTH C J, WINDHAGEN H. In vivo corrosion of four magnesium alloys and the associated bone response [J]. Biomaterials, 2005, 26: 3557−3563.

[33] ZHANG Er-lin, XU Li-ping, YU Guo-ning, PAN Feng, YANG Ke. In vivo evaluation of biodegradable magnesium alloy bone implant in the first 6 months implantation [J]. Journal of Biomedical Materials Research Part A, 2009, 90: 882−893.

[34] WITTE F. The history of biodegradable magnesium implants: A review [J]. Acta Biomaterialia, 2010, 6: 1680−1692.

[35] KISELEVSKY M V, ANISIMOVA N Y, POLOTSKY B E, MARTYNENKO N S, LUKYANOVA E A, SITDIKOVA S M, DOBATKIN S V. Biodegradable magnesium alloys as promising materials for medical applications [J]. Modern Technologies in Medicine, 2019, 11: 146−155.

[36] YASZEMSKI M J, TRANTOLO D J, LEWANDROWSKI K U, HASIRCI V, ALTOBELLI D E, WISE D L. Biomaterials in orthopedics [M]. New York: CRC Press, 2003.

[37] FONTANA M G. Corrosion engineering [M]. 3rd ed. New York: McGraw-Hill Book Company, 1986.

[38] GONZÁLEZ S, PELLICER E, SURIÑACH S, BARÓ M D, SORT J. Biodegradation and mechanical integrity of magnesium and magnesium alloys suitable for implants [C]// Biodegradation — Engineering and Technology. Rijeka: InTech, 2013: 313−340.

[39] THOMAS S, MEDHEKAR N V, FRANKEL G S, BIRBILIS N. Corrosion mechanism and hydrogen evolution on Mg [J]. Current Opinion in Solid State and Materials Science, 2015, 19: 85−94.

[40] SONG G L, ATRENS A. Corrosion mechanisms of magnesium alloys [J]. Advanced Engineering Materials, 1999, 1: 11−33.

[41] KE C, POHL K, BIRBILIS N, CHEN X B. Protective strontium phosphate coatings for magnesium biomaterials [J]. Materials Science and Technology, 2014, 30: 521−526.

[42] LIN X, TAN L L, ZHANG Q, YANG K, HU Z Q, QIU J H, CAI Y. The in vitro degradation process and biocompatibility of a ZK60 magnesium alloy with a forsterite-containing micro-arc oxidation coating [J]. Acta Biomaterialia, 2013, 9: 8631−8642.

[43] ZHAO H, CAI S, NIU S X, ZHANG R, WU X D, XU G H, DING Z T. The influence of alkali pretreatments of AZ31 magnesium alloys on bonding of bioglass–ceramic coatings and corrosion resistance for biomedical applications [J]. Ceramics International, 2015, 41: 4590−4600.

[44] GAO Y L, LIU Y, SONG X Y. Plasma-sprayed hydroxyapatite coating for improved corrosion resistance and bioactivity of magnesium alloy [J]. Journal of Thermal Spray Technology, 2018, 27: 1381−1387.

[45] RAZAVI M, FATHI M, SAVABI O, VASHAEE D, TAYEBI L. In vitro study of nanostructured diopside coating on Mg alloy orthopedic implants [J]. Materials Science and Engineering C, 2014, 41: 168−177.

[46] PRABHU D B, GOPALAKRISHNAN P, RAVI K R. Morphological studies on the development of chemical conversion coating on surface of Mg−4Zn alloy and its corrosion and bio mineralisation behaviour in simulated body fluid [J]. Journal of Alloys and Compounds, 2020, 812: 152146.

[47] PULIDO-GONZÁLEZ N, TORRES B, ZHELUDKEVICH M L, RAMS J. High Power Diode Laser (HPDL) surface treatments to improve the mechanical properties and the corrosion behaviour of Mg−Zn−Ca alloys for biodegradable implants [J]. Surface and Coatings Technology, 2020, 402: 126314.

[48] LI Jing-an, CHEN Li, ZHANG Xue-qi, GUAN Shao-kang. Enhancing biocompatibility and corrosion resistance of biodegradable Mg−Zn−Y−Nd alloy by preparing PDA/HA coating for potential application of cardiovascular biomaterials [J]. Materials Science and Engineering: C, 2020, 109: 110607.

[49] UDDIN M, HALL C, SANTOS V, VISALAKSHAN R, QIAN G T, VASILEV K. Synergistic effect of deep ball burnishing and HA coating on surface integrity, corrosion and immune response of biodegradable AZ31B Mg alloys [J]. Materials Science and Engineering: C, 2021, 118: 111459.

[50] WITTE F, FISCHER J, NELLESEN J, VOGT C, VOGT J, DONATH T, BECKMANN F. In vivo corrosion and corrosion protection of magnesium alloy LAE442 [J]. Acta Biomaterialia, 2010, 6: 1792−1799.

[51] MAO Lin, ZHU Hong-wang, CHEN Li, ZHOU Hao, YUAN Guang-yin, SONG Cheng-li. Enhancement of corrosion resistance and biocompatibility of Mg−Nd−Zn−Zr alloy achieved with phosphate coating for vascular stent application [J]. Journal of Materials Research and Technology, 2020, 9: 6409−6419.

[52] ZHENG Yu-feng, GU Xue-nan, WITTE F. Biodegradable metals [J]. Materials Science and Engineering: R, 2014, 77: 1−34.

[53] JAFARI S, HARANDI S E, SINGH RAMAN R K. A review of stress-corrosion cracking and corrosion fatigue of magnesium alloys for biodegradable implant applications [J]. JOM, 2015, 67: 1143−1153.

[54] JAFARI S, RAMAN R K S, DAVIES C H J, HOFSTETTER J, UGGOWITZER P J, LÖFFLER J F. Stress corrosion cracking and corrosion fatigue characterisation of MgZn1Ca0.3 (ZX10) in a simulated physiological environment [J]. Journal of the Mechanical Behavior of

Biomedical Materials, 2017, 65: 634−643.

[55] CHOUDHARY L, SINGH RAMAN R K. Magnesium alloys as body implants: Fracture mechanism under dynamic and static loadings in a physiological environment [J]. Acta Biomaterialia, 2012, 8: 916−923.

[56] JAFARI H, RAHIMI F, SHEIKHSOFLA Z. In vitro corrosion behavior of Mg−5Zn alloy containing low Y contents [J]. Materials and Corrosion, 2016, 67: 396−405.

[57] IDRIS M H, JAFARI H, HARANDI S E, MIRSHAHI M, KOLEYNI S. Characteristics of as-cast and forged biodegradable Mg−Ca binary alloy immersed in kokubo simulated body fluid [J]. Advanced Materials Research, 2012, 445: 301−306.

[58] HARANDI S E, MIRSHAHI M, KOLEINI S, IDRIS M H, JAFARI H, KADIR M R A. Effect of calcium content on the microstructure, hardness and in-vitro corrosion behavior of biodegradable Mg−Ca binary alloy [J]. Materials Research, 2013, 16: 11−18.

[59] LIU Bao-sheng, CAO Miao-miao, ZHANG Yue-zhong, HU Yong, GONG Chang-wei, HOU Li-feng, WEI Ying-hui. Microstructure, anticorrosion, biocompatibility and antibacterial activities of extruded Mg−Zn−Mn strengthened with Ca [J]. Transactions of Nonferrous Metals Society of China, 2021, 31: 358−370.

[60] CHOUDHARY L, SINGH RAMAN R K, NIE J F. In vitro evaluation of degradation of a calcium phosphate coating on a Mg−Zn−Ca alloy in a physiological environment [J]. Corrosion, 2012, 68: 499−506.

[61] JAFARI S, SINGH RAMAN R K. In-vitro biodegradation and corrosion-assisted cracking of a coated magnesium alloy in modified-simulated body fluid [J]. Materials Science and Engineering: C, 2017, 78: 278−287.

[62] GAUR S, SINGH RAMAN R K, KHANNA A S. In vitro investigation of biodegradable polymeric coating for corrosion resistance of Mg−6Zn−Ca alloy in simulated body fluid [J]. Materials Science and Engineering: C, 2014, 42: 91−101.

[63] SHAHRI S M G, IDRIS M H, JAFARI H , GHOLAMPOUR B , ASSADIAN M. Effect of solution treatment on corrosion characteristics of biodegradable Mg−6Zn alloy [J]. Transactions of Nonferrous Metals Society of China, 2015, 25: 1490−1499.

[64] JAFARI H, HEIDARI E, BARABI A, DASHTI KHEIRABADI M. Effect of phase transformation during long-term solution treatment on microstructure, mechanical properties, and bio-corrosion behavior of Mg−5Zn−1.5Y cast alloy [J]. Acta Metallurgica Sinica (English Letters), 2018, 31: 561−574.

[65] HARANDI S E, HASBULLAH IDRIS M, JAFARI H. Effect of forging process on microstructure, mechanical and corrosion properties of biodegradable Mg−1Ca alloy [J]. Materials & Design, 2011, 32: 2596−2603.

[66] JAFARI H, DOOST MOHAMMADI F. Effect of extrusion temperature on microstructure and biodegradation behavior of Mg−5Zn−1Y−1Ca alloy [J]. International Journal of Chemical Engineering and Applications, 2017, 8: 299−304.

[67] RAMALINGAM V V, RAMASAMY P, KOVUKKAL M D, MYILSAMY G. Research and development in magnesium alloys for industrial and biomedical applications: A review [J]. Metals and Materials International, 2020, 26: 409−430.

[68] HUMPHREYS F J, HATHERLY M. Recrystallization textures [C]//Recrystallization and related annealing phenomena. Amsterdam: Elsevier, 2004: 379−413.

[69] CHEN Yong-jun, WANG Qu-dong, PENG Jiang-guo, ZHAI Chun-quan, DING Wen-jiang. Effects of extrusion ratio on the microstructure and mechanical properties of AZ31 Mg alloy [J]. Journal of Materials Processing Technology, 2007, 182: 281−285.

[70] DU Yu-zhou, ZHENG Ming-yi, XU Chao, QIAO Xiao-guang, WU Kun, LIU Xiao-dong, WANG Guo-jun, LV Xin-yu. Microstructures and mechanical properties of as-cast and as-extruded Mg−4.50Zn−1.13Ca (wt.%) alloys [J]. Materials Science and Engineering: A, 2013, 576: 6−13.

[71] MA Li-na, YANG Yan, ZHOU Gang, REN Feng-juan, DENG Hong-ju, WEI Guo-bing, PENG Xiao-dong. Effect of rolling reduction and annealing process on microstructure and corrosion behavior of LZ91 alloy sheet [J]. Transactions of Nonferrous Metals Society of China, 2020, 30: 1816−1825.

[72] FRIEDRICH H E, MORDIKE B L. Magnesium technology —Metallurgy, design data, applications [M]. Berlin: Springer, 2006.

[73] CZERWINSKI F. Magnesium injection molding [M]. Boston, MA: Springer, 2008.

[74] CHENG Jia-hao, GHOSH S. A crystal plasticity FE model for deformation with twin nucleation in magnesium alloys [J]. International Journal of Plasticity, 2015, 67: 148−170.

[75] ASM. Properties and selection: Nonferrous alloys and special-purpose materials (Vol 2) [M]. ASM International, 2011.

[76] PEKGULERYUZ M O, KAINER I K U, ARSLAN KAYA A. Fundamentals of magnesium alloy metallurgy [M]. UK: Elsevier, 2013.

[77] SEONG J W, KIM W J. Development of biodegradable Mg−Ca alloy sheets with enhanced strength and corrosion properties through the refinement and uniform dispersion of the Mg_2Ca phase by high-ratio differential speed rolling [J]. Acta Biomaterialia, 2015, 11: 531−542.

[78] XIA Yong-hua, ZHANG Bao-ping, WANG Yin, QIAN Ming-fang, GENG Lin. In-vitro cytotoxicity and in-vivo biocompatibility of as-extruded Mg–4.0Zn–0.2Ca alloy [J]. Materials Science and Engineering: C, 2012, 32: 665−669.

[79] CHA P R, HAN H S, YANG G F, KIM Y C, HONG K H, LEE S C, JUNG J Y, AHN J P, KIM Y Y, CHO S Y, BYUN J Y, LEE K S, YANG S J, SEOK H K. Biodegradability engineering of biodegradable Mg alloys: Tailoring the electrochemical properties and microstructure of constituent phases [J]. Scientific Reports, 2013, 3: 2367.

[80] ZHONG Li-ping, WANG Yong-jian, LUO Hong, CUI Xue-jun, ZHANG Ying-jun, DOU Bao-jie, PENG Jian. Influence of aging prior to extrusion on the microstructure and corrosion resistance of Mg−8Sn−2Zn−0.2Mn alloy [J]. Journal of Alloys and Compounds, 2019, 780: 783−791.

[81] Types of extrusion process: Working, advantages & disadvantages [EB/OL]. 2022, https://engineeringlearn.com/types-of-extrusion-process-working-advantages-disadvantages/.

[82] ASM. Forming and forging (Vol 14) [M]. ASM International, 1988.

[83] WU Peng-peng, XU Fang-jun, DENG Kun-kun, HAN Fu-yin, ZHANG Zhong-zhong, GAO Rui. Effect of extrusion on corrosion properties of Mg−2Ca−χAl (χ=0, 2, 3, 5) alloys [J]. Corrosion Science, 2017, 127: 280−290.

[84] KRÜGER D, ZELLER-PLUMHOFF B, WIESE B, YI S, ZUBER M, WIELAND D C F, MOOSMANN J, WILLUMEIT-RÖMER R. Assessing the microstructure and in vitro degradation behavior of Mg−*x*Gd screw implants using μCT [J]. Journal of Magnesium and Alloys, 2021, 9: 2207−2222.

[85] WU Qiong, ZHU Shi-jie, WANG Li-guo, LIU Qian, YUE Gao-chao, WANG Jun, GUAN Shao-kang. The microstructure and properties of cyclic extrusion compression treated Mg−Zn−Y−Nd alloy for vascular stent application [J]. Journal of the Mechanical Behavior of Biomedical Materials, 2012, 8: 1−7.

[86] LU Yu, BRADSHAW A R, CHIU Yu-lung, JONES I P. Effects of secondary phase and grain size on the corrosion of biodegradable Mg−Zn−Ca alloys [J]. Materials Science and Engineering: C, 2015, 48: 480−486.

[87] BIRBILIS N, RALSTON K D, VIRTANEN S, FRASER H L, DAVIES C H J. Grain character influences on corrosion of ECAPed pure magnesium [J]. Corrosion Engineering, Science and Technology, 2010, 45: 224−230.

[88] HAN H S, MINGHUI Y, SEOK H K, BYUN J Y, CHA P R, YANG C L, KIM Y C. The modification of microstructure to improve the biodegradation and mechanical properties of a biodegradable Mg alloy [J]. Journal of the Mechanical Behavior of Biomedical Materials, 2013, 20: 54−60.

[89] ZOU Guo-dong, PENG Qiu-ming, WANG Ya-nan, LIU Bao-zhong. The effect of extension twinning on the electrochemical corrosion properties of Mg−Y alloys [J]. Journal of Alloys and Compounds, 2015, 618: 44−48.

[90] ZHENG Yang, LI Yan, CHEN Ji-hua, ZOU Zheng-yang. Effects of tensile and compressive deformation on corrosion behaviour of a Mg−Zn alloy [J]. Corrosion Science, 2015, 90: 445−450.

[91] HAMU G B, ELIEZER D, WAGNER L. The relation between severe plastic deformation microstructure and corrosion behavior of AZ31 magnesium alloy [J]. Journal of Alloys and Compounds, 2009, 468: 222−229.

[92] LI Cheng-jie, SUN Hong-fei, LI Xue-wen, ZHANG Jun-ling, FANG Wen-bin, TAN Ze-yi. Microstructure, texture and mechanical properties of Mg−3.0Zn−0.2Ca alloys fabricated by extrusion at various temperatures [J]. Journal of Alloys and Compounds, 2015, 652: 122−131.

[93] SONG G L, MISHRA R, XU Z Q. Crystallographic orientation and electrochemical activity of AZ31 Mg alloy [J]. Electrochemistry Communications, 2010, 12: 1009−1012.

[94] XIN Ren-long, WANG Mao-yin, GAO Jia-cheng, LIU Pei, LIU Qing. Effect of microstructure and texture on corrosion resistance of magnesium alloy [J]. Materials Science Forum, 2009, 610/611/612/613: 1160−1163.

[95] JIANG Bin, XIANG Qing, ATRENS A, SONG Jiang-feng, PAN Fu-sheng. Influence of crystallographic texture and grain size on the corrosion behaviour of as-extruded Mg alloy AZ31 sheets [J]. Corrosion Science, 2017, 126: 374−380.

[96] FAN Jun, QIU Xin, NIU Xiao-dong, TIAN Zheng, SUN Wei, LIU Xiao-juan, LI Yang-de, LI Wei-rong, MENG Jian. Microstructure, mechanical properties, in vitro degradation and cytotoxicity evaluations of Mg−1.5Y−1.2Zn−0.44Zr alloys for biodegradable metallic implants [J]. Materials Science and Engineering: C, 2013, 33: 2345−2352.

[97] ZHOU Y L, LI Y, LUO D M, DING Y. Influence of extrusion on the microstructure, mechanical properties and in vitro corrosion performance of biodegradable Mg−1Mn−2Zn−1Nd alloy [J]. Materials Technology: Advanced Performance Materials, 2016, 31: 585−589.

[98] ZHENG Xing-wei, DONG Jie, XIANG Ya-zhen, CHANG Jian-wei, WANG Feng-hua, JIN Li, WANG Ying-xin, DING Wen-jiang. Formability, mechanical and corrosive properties of Mg–Nd–Zn–Zr magnesium alloy seamless tubes [J]. Materials & Design, 2010, 31: 1417−1422.

[99] BAEK S M, KANG J S, KIM J C, KIM B, SHIN H J, PARK S S. Improved corrosion resistance of Mg–8Sn–1Zn–1Al alloy subjected to low-temperature indirect extrusion [J]. Corrosion Science, 2018, 141: 203−210.

[100] MOHAMMADI F D, JAFARI H. Microstructure characterization and effect of extrusion temperature on biodegradation behavior of Mg−5Zn−1Y−*x*Ca alloy [J]. Transactions of Nonferrous Metals Society of China, 2018, 28: 2199−2213.

[101] BEN-HAROUSH M, BEN-HAMU G, ELIEZER D, WAGNER L. The relation between microstructure and corrosion behavior of AZ80 Mg alloy following different extrusion temperatures [J]. Corrosion Science, 2008, 50: 1766−1778.

[102] MIAO Jiao, YE Bing, WANG Qu-dong, PENG Tao. Mechanical properties and corrosion resistance of Mg−10Gd−2Y−0.5Zr alloy by hot extrusion solid-state recycling [J]. Journal of Alloys and Compounds, 2013, 561: 184−192.

[103] LI Jun-lei, TAN Li-li, WAN Peng, YU Xiao-ming, YANG Ke. Study on microstructure and properties of extruded Mg−2Nd−0.2Zn alloy as potential biodegradable implant material [J]. Materials Science and Engineering: C, 2015, 49: 422−429.

[104] ZHOU S J, LIU L, HUANG N. Effect of extrusion ratio on microstructure, mechanical and degradation properties of Mg−2Zn−0.2Mn biomedical alloy [J]. Integrated Ferroelectrics, 2014, 154: 166−174.

[105] XU Hong, ZHANG Xin, ZHANG Kui, SHI Yang, REN Ji-ping. Effect of extrusion on corrosion behavior and corrosion mechanism of Mg−Y alloy [J]. Journal of Rare Earths, 2016, 34: 315−327.

[106] ZHANG Tie-lei, JI Ze-sheng, WU Shu-yan. Effect of extrusion ratio on mechanical and corrosion properties of AZ31B alloys prepared by a solid recycling process [J]. Materials & Design, 2011, 32: 2742−2748.

[107] ATRENS A, SHI Zhi-ming, MEHREEN S U, JOHNSTON S, SONG Guang-ling, CHEN Xian-hua, PAN Fu-sheng. Review of Mg alloy corrosion rates [J]. Journal of Magnesium and Alloys, 2020, 8: 989−998.

[108] RALSTON K D, BIRBILIS N. Effect of grain size on

corrosion: A review [J]. Corrosion, 2010, 66: 1−13.
[109] ATRENS A, SONG G L, CAO F Y, SHI Z M, BOWEN P K. Advances in Mg corrosion and research suggestions [J]. Journal of Magnesium and Alloys, 2013, 1: 177−200.
[110] BIRBILIS N, ZHANG M X, ESTRIN Y. Surface grain size effects on the corrosion of magnesium [J]. Key Engineering Materials. 2008, 384: 229−240.
[111] ZHANG Wen, TAN Li-li, NI Ding-rui, CHEN Jun-xiu, ZHAO Ying-chao, LIU Long, SHUAI Ci-jun, YANG Ke, ATRENS A, ZHAO Ming-chun. Effect of grain refinement and crystallographic texture produced by friction stir processing on the biodegradation behavior of a Mg−Nd−Zn alloy [J]. Journal of Materials Science & Technology, 2019, 35: 777−783.
[112] TONG Li-bo, ZHENG Ming-yi, CHENG Li-ren, KAMADO S, ZHANG Hong-jie. Effect of extrusion ratio on microstructure, texture and mechanical properties of indirectly extruded Mg−Zn−Ca alloy [J]. Materials Science and Engineering A, 2013, 569: 48−53.
[113] WANG Yan-peng, LI Feng, WANG Ye, LI Xue-wen, FANG Wen-win. Effect of extrusion ratio on the microstructure and texture evolution of AZ31 magnesium alloy by the staggered extrusion (SE) [J]. Journal of Magnesium and Alloys, 2020, 8: 1304−1313.
[114] CAO Fu-yong, SONG Guang-ling, ATRENS A. Corrosion and passivation of magnesium alloys [J]. Corrosion Science, 2016, 111: 835−845.
[115] ATRENS A. Revolutionising biodegradable biomaterials—Significance of Magnesium and its alloys [M]. Oxford: Woodhead Publishing, 2015: 3−28.

挤压参数对生物植入应用镁合金降解性能的影响：综述

Mahdi SHIRI[1], Hassan JAFARI[1], Raman SINGH[2]

1. Materials Engineering Department, Faculty of Materials Engineering and Interdisciplinary Sciences, Shahid Rajaee Teacher Training University (SRTTU), 16785-136 Tehran, Iran;
2. Department of Mechanical & Aerospace Engineering and Department of Chemical Engineering, 17 College Walk (Bldg 31), Monash University-Clayton Campus (Melbourne), Vic 3800, Australia

摘　要：作为新一代临时生物材料，镁合金具有良好的生物相容性和生物可降解性，也有助于损伤骨组织的修复。但是，其在人体体液中不具备所要求的耐腐蚀性能。挤压等热机械加工对镁合金的力学性能和生物腐蚀行为均有影响。本文综述挤压参数(挤压比和温度)对镁合金生物腐蚀性能的影响。它们的影响主要归因于挤压合金显微组织的改变，包括最终的晶粒尺寸和均匀度、织构以及第二相的尺寸、分布和体积分数。挤压过程中的动态再结晶和晶粒细化使组织更均匀，并导致基面织构的形成，从而提高镁合金的强度和耐腐蚀性能。挤压温度和挤压比是影响降解的重要因素。随着挤压比的增加和/或挤压温度的降低，镁合金的晶粒尺寸减小，与挤压方向平行的样品两侧的基面织构增强，析出相体积分数降低，晶粒尺寸减小，这些都有助于提高镁合金植入物的耐腐蚀性能。

关键词：镁合金；挤压温度；挤压比；生物降解；显微组织

(Edited by Xiang-qun LI)